Coral Reefs
https://doi.org/10.1007/s00338-026-02892-1

RESEARCH

Large-scale carbon storage in the deep-sea through cold-water coral mounds off the Campeche Bank, Gulf of Mexico

L. Greiffenhagen[1] · J. Titschack[1] · C. Wienberg[1] · L. H. De Clippele[2] · L. Matos[3] · J. Gafeira[4] · A. Schröder-Ritzrau[5] · K. Arul[5] · N. Frank[5] · D. Hebbeln[1,6]

Received: 16 September 2025 / Accepted: 13 May 2026

Abstract Reef-building cold-water corals form large seabed structures known as coral mounds. As demonstrated in studies from the Northeast Atlantic and Mediterranean Sea, coral mounds accumulate large amounts of carbon(ate). However, beyond the scale of individual mounds, long-term accumulation of both organic (C_{org}) and inorganic carbon (C_{inorg}) at the mound province scale remains poorly quantified. In this study, we investigate the Campeche Mound Province, southern Gulf of Mexico, which consists of interconnected coral mound ridges covering an area of > 40 km^2. Using sediment cores, we reconstruct total carbon (C_{org} and C_{inorg}) accumulation in the Campeche Mounds over the past ~ 250 kyr. The results show mean total carbon accumulation rates of 0.5–5.6 g C cm^{-2} kyr^{-1}. This is three to nine times higher than on the surrounding seafloor. We then upscale obtained carbon concentration data to the entire mound province using high-resolution bathymetry and the CoMMa toolbox, a novel morphometric mapping tool. The total carbon storage of the Campeche Mounds amounts to an estimated 18.5 megatons of carbon that is transferred to the long-term carbon cycle and immobilised for millions of years. For the first time, we present a combination of core-based analysis and spatial mapping. Through accounting for different approaches and time scales, we provide reliable value ranges for carbon accumulation rates in coral mounds. The Campeche Mound Province is not fully mapped and likely much larger, highlighting the substantial, albeit overlooked long-term carbon burial through benthic deep-sea ecosystems in the southern Gulf of Mexico and beyond.

Abstracta Los corales de aguas frías constructores de arrecifes forman grandes estructuras en el lecho marino conocidas como montes de coral (coral mounds). Como demuestran estudios realizados en el Atlántico nororiental y el Mediterráneo, los montes de coral acumulan grandes cantidades de carbon(at)o. Sin embargo, más allá de la escala de los montes individuales, la acumulación a largo plazo de carbono orgánico (C_{org}) e inorgánico (C_{inorg}) a escala de provincia de montes de coral sigue estando poco cuantificada. En este estudio, investigamos la Provincia de Montes de Coral de Campeche, al sur del Golfo de México, que consiste en crestas de montes de coral interconectados que cubren un área de > 40 km^2. Utilizando núcleos de sedimentos, reconstruimos la acumulación total de carbono (C_{org} y C_{inorg}) en los montes de coral de Campeche durante los últimos ~ 250 ka. Los resultados muestran tasas medias de acumulación de carbono total de 0.5–5.6 g C cm^{-2} ka^{-1}. Esto es entre tres y nueve veces más rápido que en el fondo marino circundante. También, ampliamos los datos de concentración de carbono obtenidos a toda la provincia de montes de coral utilizando batimetría de alta resolución y la

Supplementary Information The online version contains supplementary material available at https://doi.org/10.1007/s00338-026-02892-1.

✉ L. Greiffenhagen
lgreiffenhagen@marum.de

[1] MARUM – Center for Marine Environmental Sciences, University of Bremen, Bremen, Germany

[2] School of Biodiversity, One Health & Veterinary Medicine, University of Glasgow, Glasgow, UK

[3] Centro de Ciências do Mar do Algarve (CCMAR/CIMAR LA), Universidade Do Algarve, Campus de Gambelas, Faro, Portugal

[4] Kelpie Geoscience Ltd., Enterprise Hub, 10 Max Born Crescent, Edinburgh, UK

[5] IUP Institute of Environmental Physics, University of Heidelberg, Heidelberg, Germany

[6] Faculty of Geosciences, University of Bremen, Bremen, Germany

Published online: 03 August 2026

CoMMa toolbox, una novedosa herramienta de cartografía morfométrica. El almacenamiento total de carbono de los montes de coral de Campeche asciende a unas 18,5 megatoneladas de carbono que se transfiere al ciclo del carbono a largo plazo y se inmoviliza durante millones de años. Por primera vez, presentamos una combinación de análisis basados en núcleos de sedimentos y cartografía espacial. Al tener en cuenta diferentes enfoques y escalas temporales, proporcionamos rangos de valores más fiables para las tasas de acumulación de carbono en los montes de coral. La Provincia de los Montes de Coral de Campeche no está totalmente cartografiada y es probable que sea mucho mayor de lo que se conoce, lo cual resalta la importancia—aunque hasta ahora poco reconocida—del enterramiento de carbono a largo plazo a través de los ecosistemas bentónicos de aguas profundas en el sur del Golfo de México y más allá.

Keywords Cold-water coral reefs · Carbon accumulation · Carbon storage · Reef sediments · Habitat mapping · Coral mounds

Introduction

The quantification of marine carbon pathways is crucial to understanding the earth system and the consequences of a rapidly changing global climate (e.g. Friedlingstein et al. 2025). While pelagic processes and carbon pathways in the short-term carbon cycle (atmosphere-hydrosphere-biosphere) are better understood, the role of deep benthic ecosystems in the transfer of carbon between the short-term and long-term carbon cycle remains poorly quantified (e.g. Wood et al. 2023; Schultz et al. 2025). This process, known as carbon accumulation, refers to the transfer of carbon from the active reservoir (10s–10^3s years) to the inactive reservoir (lithosphere; >> 10^3s years; Cartapanis et al. 2018) through benthic carbon burial. Only recently, cold-water coral (CWC) reefs were identified as some of the most extensive benthic ecosystems of the deep-sea that exist along a wide latitudinal and water depth range (Freiwald et al. 2004) and equally as considerable carbonate factories (sensu Schlager 2003; Reijmer 2021).

Cold-water coral reefs can persist for thousands of years and build large topographic features on the seabed, known as coral mounds (Roberts et al. 2009; Wienberg and Titschack 2017). These mounds are composed of carbonate coral framework and baffled fine-grained sediment (Wang et al. 2021). They develop through alternating cycles of reef growth and extinction (i.e. active vs. inactive mound formation), controlled by a certain set of environmental conditions (Wienberg and Titschack 2017; Hebbeln et al. 2019a). Over geological timescales, coral mounds can rise tens to hundreds of metres above the seabed and can exceed one million years in age (Mienis et al. 2006; Kano et al. 2007). Coral mounds are widespread along the continental margins of the Atlantic (see Cordes and Mienis, 2023 and references therein), as well as in its marginal seas, the Mediterranean Sea (Corbera et al. 2019; Fink et al. 2013), and the Gulf of Mexico (Mienis et al. 2012; Hebbeln et al. 2014; Roberts and Kohl 2018).

During their active state, coral mounds can reach high aggradation rates (up to > 100 cm kyr^{-1}; e.g. Wienberg & Titschack 2017), leading to rapid accumulation of carbonate (inorganic carbon): this involves the coral carbonate framework, as well as hemipelagic and benthic carbonates contributing to the mound sediments (e. g. Titschack et al. 2009). Additionally, coral mounds accumulate organic carbon (C_{org}), suggesting that coral mounds may be hotspots of total carbon ($C_{inorg} + C_{org}$) accumulation (Greiffenhagen et al. 2025a). Total carbon accumulation is here defined as the net burial of all carbon sources, including material export from the water column to the seafloor and in situ reef-production, minus dissolution and erosion (e.g. Wood et al. 2023; Courtney and Andersson 2025). While multiple carbon-related dynamics happen around and within a CWC reef (e.g. De Clippele et al. 2021a,b; Maier et al. 2023), such as organic matter influx and metabolism (short-term carbon reservoir), the carbon accumulation refers to the material that is being buried in situ into the long-term carbon reservoir (> 10 kyr). This reservoir is herein defined as the carbon storage. In order to understand the role of coral mounds in the carbon cycle, the quantification of this process, i.e. carbon(ate) accumulation in coral mounds across time and space, is essential. Only a few localised studies have addressed this particular question in detail with regard to coral mounds (Dorschel et al. 2007; Titschack et al. 2009, 2015, 2016; Edinger et al. 2025; Greiffenhagen et al. 2025a). These sediment core-based studies found carbonate accumulation rates of up to > 100 g $CaCO_3$ cm^{-2} kyr^{-1} (Titschack et al. 2015, 2016). Depending on location and time scale analysed, the rates have a wide range, and can also be much lower (< 0.3–17 g $CaCO_3$ cm^{-2} kyr^{-1}; Dorschel et al. 2007; Titschack et al. 2009; Edinger et al. 2025). Recently, the total carbon accumulation on a coral mound was quantified for the first time, showing that both C_{inorg} and C_{org} accumulation can occur at rates > 10 times higher than on the surrounding seabed, and at the same scale as other carbon-storing ecosystems (Greiffenhagen et al. 2025a). However, the existing studies are limited to specific time periods and individual mounds.

Taking a different approach, mapping-based spatial studies have estimated that the absolute amount of carbon(ate) stored in large coral mound provinces off Norway, Morocco and Namibia is regionally considerable (Lindberg & Mienert 2005; Hebbeln et al. 2019b; Tamborrino et al. 2022). These upscaling-approaches are yet limited by either simplified assumptions about mound quantity, shapes and volume, or lack locally derived carbon(ate) accumulation data. Consequently, the role and significance of coral mounds in the carbon cycle is still lacking a comprehensive understanding, and cannot be integrated appropriately into global carbon budget calculations (see Smith and Mackenzie 2016; Woods et al. 2023). Thorough, multi-point assessments of carbon accumulation dynamics over time, as well as suitable and representative spatial upscaling techniques, are necessary to advance this field of research. Further, our knowledge is geographically limited to coral mound sites in the eastern Atlantic and Mediterranean Sea, while carbonate accumulation studies are missing in the western Atlantic, despite the widespread occurrence of large mound provinces there (e.g. Correa et al. 2012; Steinmann et al. 2020; Raddatz et al. 2020; Sowers et al. 2024).

One example is the Campeche Mound Province, southern Gulf of Mexico, where ridge-shaped coral mounds with heights of 20–40 m rise from water depths of 500–600 m (Hübscher et al. 2010; Hebbeln et al. 2014) at the eastern margin of the Campeche Bank, a carbonate shelf that is connected to the Yucatan Peninsula, Mexico (Wilhelm and Ewing 1972). Stretching beyond a mapped area of 40 km^2, the Campeche Mounds comprise the largest known coral mound province within the Gulf of Mexico (Hebbeln et al. 2014; Brooke et al. 2023). The Campeche Mounds are associated with contourite drift deposits in an oceanographic setting characterised by strong bottom currents (Hebbeln et al. 2016), localised upwelling (i.e. high-productivity; Merino 1997; Reyes-Jiménez et al. 2023) and internal wave activity along the pycnocline between the Tropical Atlantic Central Water and the Antarctic Intermediate Water (Hebbeln et al. 2014; Meunier et al. 2023). Together, the sufficient availability and delivery of food (organic matter) generate suitable conditions for a thriving CWC reef ecosystem, which is largely dominated by colonies of the framework-building scleractinian CWCs *Lophelia pertusa (*syn. *Desmophyllum pertusum)* and *Enallopsammia profunda* (Hebbeln et al. 2014). Matos et al. (2017) provided evidence for reoccurring mound formation (i.e. active reef growth) on the Campeche Mounds since > 250 kyr ago, mainly restricted to interglacial periods (marine isotope stage MIS7, 5, 1). While mound formation stagnated during the entire last glacial, the reefs on the Campeche Mounds have been thriving since ~ 10 kyr BP, and therefore accumulating carbon.

Here, we aim to provide the first detailed study investigating both the temporal scale of carbon accumulation and the spatial scale, i.e. total amount of carbon stored within the Campeche Mound Province. This combination is made possible through the analysis and combination of sediment cores (temporal integration of carbon accumulation) and bathymetry data (spatial integration of carbon accumulation across the coral mound province). By upscaling multiple detailed carbon accumulation records to an approximation of total carbon storage, we provide the first numbers of carbon accumulation and large-scale storage across the Campeche Mounds. Ultimately, we then discuss their role in deep-sea benthic carbon storage.

Firstly, we (1) increase the age resolution of the Campeche Mounds' development by dating corals from multiple locations and periods of mound formation. Secondly (2), combining the age models with measurements of carbon content, we determine total carbon (organic + inorganic) accumulation rates for the last ~ 250 kyr. For comparability, we thereby (3) also compare the effectiveness of carbon accumulation relative to a core record from the adjacent seafloor. Finally, we (4) extrapolate our results to the total mapped area of the Campeche Mound Province by utilising a newly developed tool, the CoMMa toolbox (Gafeira et al. 2024), that allows us to obtain 3D mound volumes, and thus, the total amount of carbon stored.

Material and methods

Core material

Five gravity cores were collected from the Campeche Mound Province (Campeche Bank, southern Gulf of Mexico) during the RV MARIA S. MERIAN cruise MSM20-4 (Hebbeln et al. 2012). One off-mound core *GeoB16320-2* was retrieved from a sediment drift deposit slightly downslope of the coral mounds at a water depth of 626 m (Fig. 1). This core has already been intensively studied by Matos et al. (2017) and Portilho-Ramos et al. (2022) to reconstruct the palaeoceanographic conditions in the area and to link them to coral mound formation phases. For this study, the core is used to compare carbon accumulation between the off-mound environment and the Campeche Mounds.

Four on-mound cores, all composed of CWC fragments embedded in fine sediments, were taken from three different coral mounds within the Campeche Mound Province at depths ranging from 556 to 579 m (Table 1; Fig. 1). Cores *GeoB16310-2* and *GeoB16310-3* were taken from the same coral mound (*Ixchel* Mound), only a few metres apart. Core *GeoB16313-2* was taken from a coral mound (*Ah Xoc* Mound) further north, and core *GeoB16318-1* from a coral mound (*Chaac* Mound) in the southern part of the Campeche Mound Province (Fig. 1).

We combined data published by Matos et al. (2017; 25 $^{230}Th/U$ coral ages obtained from on-mound cores GeoB16310-3, GeoB16313-2, GeoB16318-1; stable oxygen isotopes and five accelerator mass spectrometry (AMS) ^{14}C ages obtained from off-mound core GeoB16320-2) with an array of newly obtained data (see Table 1), following the same approach as presented in Greiffenhagen

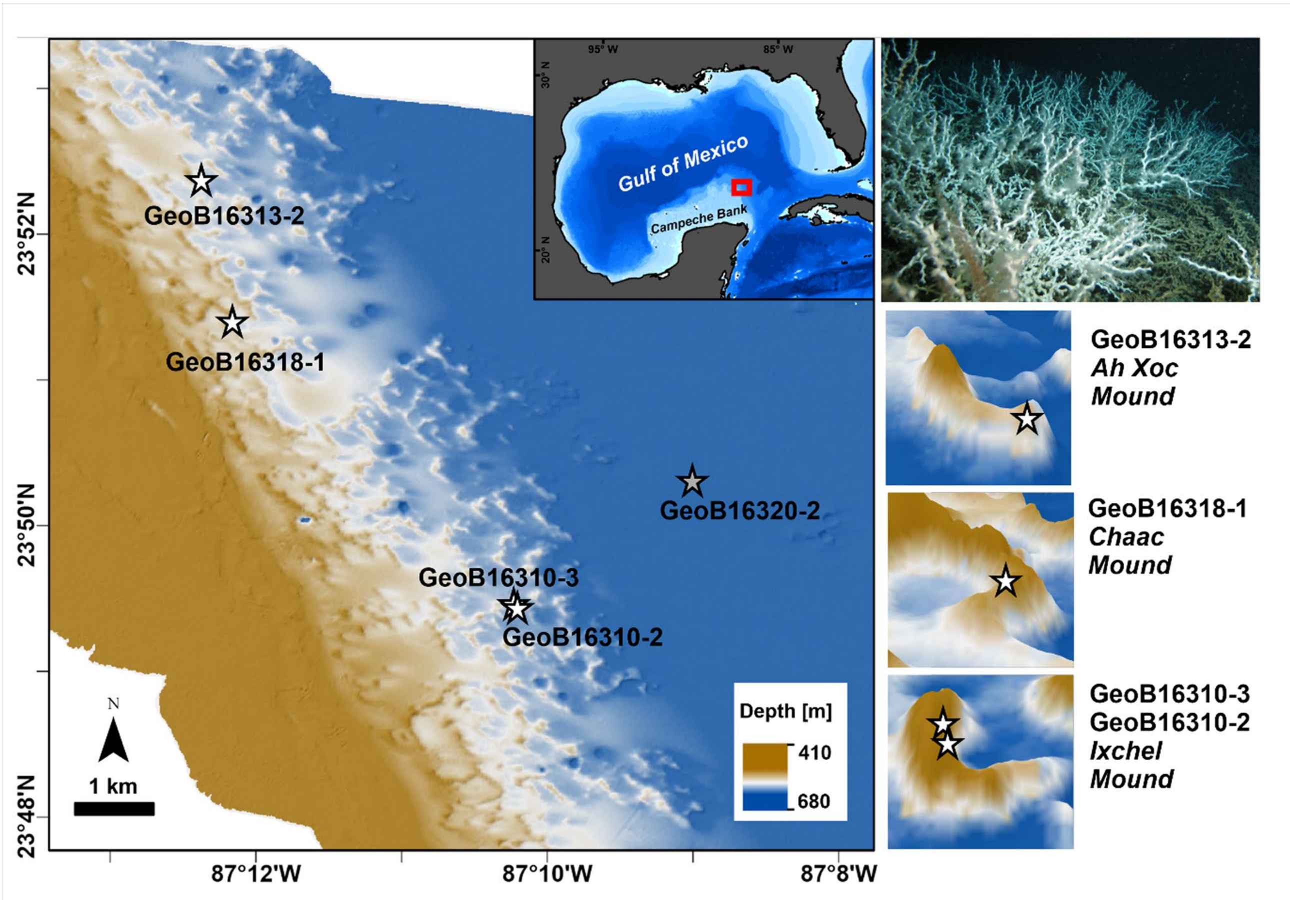

Fig. 1 Left: Map of the Campeche Mound Province (based on MBES data collected during RV MARIA S. MERIAN expedition MSM20-4; Wintersteller & Eberli, 2019). The location of the Campeche Mounds within the Gulf of Mexico is indicated by the red box in the overview map (based on GEBCO 2024). White stars indicate locations of on-mound cores collected from coral mounds in the Campeche Mound Province, the grey star indicates the location of the off-mound sediment core. Right: Remotely operated vehicle (ROV) image showing dense live cold-water coral reef framework (mainly *Lophelia pertusa*) covering the Campeche Mounds (copyright MARUM ROV Cherokee, Bremen, Germany). Each of the studied coral mounds (Ixchel, Ah Xoc and Chaac) is shown in a 3D illustration, core positions are indicated by stars. Note that for optimal visualisation, colour map symbology was subjected to dynamic depth range adjustment for the 3D illustrations

et al. (2025a): By using ^{230}Th/U dating of coral fragments, computed tomography (CT) scan-based volumetric data of coral carbonate, as well as dry bulk density and $C_{org}/_{inorg}$ content measurements from sediments, *total carbon (mass) concentration* and *accumulation* on the coral mounds were calculated.

Computed tomography scanning of on-mound cores

In order to derive coral and sediment contents within the coral mounds, we performed a volumetric core quantification of all coral mound records (GeoB16310-2, GeoB16310-3, GeoB16313-2 and GeoB16318-1) through CT scans. Cores were scanned at Klinikum Bremen-Mitte (Bremen, Germany) using a Toshiba Aquilion 64 computer tomograph, as well as a Philips Brilliance iCT Elite 256 computer tomograph. Images were reconstructed using Toshiba's patented helical cone beam reconstruction technique, as well as the filtered Back Projection and bone kernel, respectively. Further technical details are given in the metadata description of the openly available CT scan data sets (see Titschack et al. 2025a, b, c; Greiffenhagen et al. 2025b). Data were processed with the ZIB edition of Amira Software (Ver. 2024.11; Stalling et al. 2005), closely following the methodology of Titschack et al. (2015; 2016). Macrofossils were quantified by a marker-based watershed segmentation (in volume per cent: vol.%) in the *Segmentation Editor*, with markers set using threshold segmentation (*Contour-Tree Segmentation*) and quantified with the *Material Statistics* Module. Since the macrofossils consist predominantly of CWCs, we refer to them as “coral content” in the following (sensu Titschack et al. 2016). The sediment in which

Table 1 Sediment cores used for this study were collected during RV MARIA S. MERIAN expedition MSM20-4

Core ID	Description	Location [lat / lon]	Water depth [m]	Core Recovery [m]	^{230}Th/U or AMS ^{14}C dating	DBD	TIC/TOC	CT scan
GeoB16310-2	Ixchel Mound	23°49.443' N 87°10.217' W	565	4.95	13	6	15	x
GeoB16310-3	Ixchel Mound	23°49.450' N 87°10.220' W	573	10.56	8 (16)	11	23	x
GeoB16313-2	Ah Xoc Mound	23°52.365' N 87°12.373' W	556	2.51	1 (4)	3	6	x
GeoB16318-1	Chaac Mound	23°51.399' N 87°12.160' W	579	4.67	5 (6)	6	25	x
GeoB16320-2	Off Mound	23°50.305' N 87°09.003' W	626	4.39	(5)	15	34	n/a

Number of samples / data points available for each core is indicated. ^{230}Th/U coral ages and CT scans were obtained from the four on-mound cores collected from the Campeche cold-water coral mounds Ixchel, Ah Xoc and Chaac (this study; Matos et al. 2017). Previously published number of ^{230}Th/U coral ages obtained from three of the four on-mound cores and accelerator mass spectrometry (AMS) ^{14}C ages obtained from the off-mound core (Matos et al. 2017) are given in brackets. Dry bulk density (DBD) and total inorganic and organic carbon (TIC/TOC) were obtained for all cores (this study)

the macrofossils are embedded is referred to as sediment matrix. Additionally, the mean X-ray attenuation in Hounsfield units (HU) is computed. Using the same approach as Greiffenhagen et al. (2025a), running average values with a 5 cm core interval thickness were extracted from the high-resolution scan data (0.3 mm resolution) at the central slice position to best represent the core depth of interest, ending up with > 400 data points for the volumetric data of the on-mound cores.

^{230}Th/U Dating of cold-water corals

A total of 27 well-preserved fragments of the CWC species *L. pertusa* and *E. profunda* were collected at strategically picked core depths from all four on-mound gravity cores (see Table 1). The coral fragments were mechanically and chemically cleaned following Frank et al. (2004), and ^{230}Th/U dated according to the procedures described in Wefing et al. (2017). Sample preparation, chemical purification of the Th and U fractions, and mass spectrometric analyses were carried out at the Institute for Environmental Physics (IUP, University of Heidelberg, Germany) using a multi-collector inductivity coupled plasma mass spectrometer (ThermoFisher Neptune plus). The ages were obtained based on decay constants from Cheng et al. (2013), and age correction was performed according to the "Ghost Signal" correction (Kerber et al. 2023; 2025). Absolute ^{230}Th/U dates are reported as kiloyears before present (kyr BP, present = 1950). The new ages were combined with 26 coral ages previously published by Matos et al. (2017; see Table 1) to improve the on-mound core age models by more precisely defining the boundaries (i.e. hiatuses) between distinct coral age clusters that represent individual mound formation phases within each core (MFPs, see Wienberg et al. 2018; 2022). Thereby, the hiatuses represent stratigraphic periods of reef extinction, i.e. without any mound formation.

Age models of coral mound records

Coral mound aggradation rates (given in cm kyr^{-1}) for each MFP were calculated using linear interpolation between the oldest and youngest ^{230}Th/U ages of each age cluster, combined with the top and bottom core depth of the corresponding MFP (following the approach presented by Wienberg et al. 2018, 2022). Boundaries between the different MFPs were defined by a combination of coral age information and abrupt changes in CT mean x-ray attenuation or visible changes in sediment colour following the approach of Greiffenhagen et al. (2025a). Supporting information is provided in Suppl. mat. I. Since the Campeche Mounds are currently covered by thriving CWC reefs (Hebbeln et al. 2014; see Fig. 1), the top depth of the youngest MFP, corresponding to the Holocene was defined to be at 0 cm for each core.

Update of the age model of the off-mound core

The age model from Matos et al. (2017) for the off-mound core GeoB16320-2 was updated by (i) recalibrating the AMS ^{14}C ages with the Palaeo Data View software (PDV; Langner and Mulitza 2019) using the IntCal20 calibration curve (Reimer et al. 2020) and the reservoir age model of Butzin et al. (2017) and (ii) re-calculating the age model and sedimentation rates (SRs; given in cm kyr^{-1}) with Bacon (Blaauw and Christen 2011; in PDV), including the six visual correlation tie points of Matos et al. (2017).

Total organic and inorganic carbon analysis

A total of 69 sediment samples collected from the four on-mound cores and 34 from the off-mound core were analysed for total C_{inorg} and C_{org} contents (TIC/TOC; Table 1). Prior to the measurements, macrofossil fragments of ca. > 2 mm were removed from the sample material, to ascertain that the measurements are representative of the "sediment matrix" previously determined in the CT analysis. Samples were freeze-dried, ground and then measured for TIC/TOC content at the Department of Geosciences, University of Bremen (Germany) using a LECO CS 744. For each sediment sample, a sub-sample of approximately 100 mg was measured for total carbon content (TC), while a second sub-sample was first treated with hydrochloric acid to remove C_{inorg} (TIC) before the TOC content was measured. The TIC content was calculated as TIC = TC–TOC. The results of the TIC/TOC analyses represent the sediment-derived C_{inorg} and C_{org} fraction, hereafter referred to as C_{inorg} and C_{org} content in weight per cent (wt.%).

Matrix sediment dry bulk density measurements

All on-mound cores were sampled for dry bulk density (DBD) measurements at an equal distance interval of ~ 1 m ($n = 26$; see Table 1). For off-mound core GeoB16320-2, DBD samples were taken at a 30 cm-interval ($n = 15$). According to ODP standards (Blum 1997), DBD was determined based on wet-weight, dry-weight and volume measurements of each sample. Samples were dried for 24 h at 105 °C and then, after cooling down, the volumes were determined using a PentaPyc 5200e gas pycnometer (Quantachrome instruments) in the Geotechnical Laboratory at MARUM, University of Bremen (Germany).

All on-mound core DBD data were then set in relation to the mean CT X-ray attenuation data (proven as a proxy for sediment density; Orsi et al. 1994) at the same core depth (see Greiffenhagen et al. 2025a). Based on a regression function between both data sets (correlation of $R^2 = 0.97$), DBD was recalculated from the CT x-ray attenuation to significantly increase the DBD resolution (for more details, see Suppl. mat. II and III). Composed of fine sediments throughout, the off-mound core naturally has a much less complex density distribution than the on-mound cores (containing varying contents of coral fragments). Accordingly, for the case of the off-mound core, pycnometer-based DBD data points were linearly interpolated to fit the resolution of the respective off-mound C_{org} and C_{inorg} data.

Calculation of carbon accumulation

The calculation of the *total carbon accumulation* [g C cm^{-2} kyr^{-1}] is determined from the three different carbon fractions, i.e. sources: (1) the *coral inorganic carbon accumulation* (coral C_{inorg} Acc), specific to the on-mound cores, (2) the *sediment inorganic carbon accumulation* (sediment C_{inorg} Acc), and (3) the *sediment organic carbon accumulation* (sediment C_{org} Acc). These are obtained using the following formulas and units:

$$\text{coral } C_{inorg}\text{Acc} = \text{CT coral Vol.\%} \times \text{Coral Density } \frac{g}{cm^3} \times \text{Aggradation Rate} \frac{cm}{kyr} \times \frac{12.01}{100.09} \quad (1)$$

For (1), a coral density of the CWC *Lophelia pertusa* is needed. Dorschel et al. (2007) and Lunden et al. (2013) provided mean values of 2.66 g cm^{-3} from the NE Atlantic and 2.81 g cm^{-3} from the Northern Gulf of Mexico, respectively. For the calculation here, the lower value of 2.66 g cm^{-3} was chosen as conservative estimate and multiplied with the mean coral content as volumetric fraction derived from the CT analyses for each specific MFP. Aggradation rates are based on the age models of the respective cores.

$$\text{sed. } C_{inorg} \text{ Acc} = \text{TIC wt.\%} \times \text{CT sed.Vol.\%} \times \text{sed. Density} \frac{g}{cm^3} \times \text{Aggradation Rate} \frac{cm}{kyr} \quad (2)$$

$$\text{sed. } C_{org} \text{ Acc} = \text{TOC wt.\%} \times \text{CT sed.Vol.\%} \times \text{sed. Density} \frac{g}{cm^3} \times \text{Aggradation Rate} \frac{cm}{kyr} \quad (3)$$

For (2) and (3), sediment density is represented by the sediment DBD data. Further, the volumetric share of the sediment matrix (total volume minus coral volume) needs to be accounted for. The off-mound record's accumulation is equally calculated through (2) and (3), but using the SRs, DBD and carbon contents from GeoB16320-2, without the necessity to define two volumetric fractions, i.e. 100% sediment.

Total carbon accumulation rates (1 + 2 + 3) for the four on-mound cores are presented as mean per MFP. Total accumulation rates were calculated by adjusting the CT-based coral C_{inorg} data points to the data point resolution of the sediment C_{org}/C_{inorg} measurements. Total carbonate accumulation is determined by conversion of the C_{inorg} fraction (1 + 2) based on the molecular weight ratio of C_{inorg} within calcium carbonate ($CaCO_3$) of 12.01:100.09, and vice-versa to convert the coral density in (1), i.e. ~ 100% carbonate, to C_{inorg}. To allow for a comparison between on- and off-mound records, rates for the off-mound core were calculated using the time intervals corresponding to the MFPs documented in the on-mound cores. All raw off-mound data beyond the temporal MFP limits, and the raw on-mound data are provided in Suppl. mat. III and IV.

Estimation of carbon storage

To prepare the data obtained from the core records for volumetric 3D upscaling, (4) the mass carbon per volume, here defined as the *total carbon (mass) concentration*, was equally calculated for each MFP.

$$\text{tot. C concentration} = \left[(\text{TOC} + \text{TIC wt.\%}) \times \text{sed. Density}\,\frac{g}{\text{cm}^3} \times \text{CT sed.Vol.\%}\right] + \left[\text{CT coral Vol.\%} \times \text{Coral Density}\,\frac{g}{\text{cm}^3} \times \frac{12.01}{100.09}\right] \quad (4)$$

The values from the sediment C_{inorg} and C_{org} measurements, as well as the coral C_{inorg} fraction, were multiplied by their density, as outlined above, and added up, bearing in mind their share in vol.% given by the CT scan data. Results are provided in g C cm^{-3}. Based on that, the mean total carbon concentration was calculated by averaging all data points across time and space (each location and MFP) to get a representative value for the entire Campeche Mound Province. To obtain the total carbon storage, this value must be multiplied by the volume of the Campeche Mounds.

The determination of coral mound volumes is based on the multibeam echosounder (MBES) bathymetry data (resolution of 10 × 10 m) collected during the RV MARIA S. MERIAN expedition MSM20-4 (data: Wintersteller and Eberli 2019) and was performed using the *Confined Morphologies Mapping (CoMMa) Toolbox Ver. 1.2* (Gafeira et al. 2024; Arosio et al. 2024a), which was adapted from an earlier ArcMap tool (Gafeira et al. 2012, 2018; De Clippele et al. 2017). CoMMa is a novel python-based toolbox for ArcGIS Pro to semi-automatically map and quantitatively characterise seabed features such as coral mounds (De Clippele et al. 2017; Arosio et al. 2024a, b). The quantification of the coral mound volumes through CoMMa is based on four steps:

(1) *Data preparation:* To remove noise and minimise the significance of anomalous pixels, the bathymetry data set was smoothened, using the low-pass filter provided by CoMMa, which re-calculates the average value for each 3 × 3 pixel neighbourhood (Arosio et al. 2024a).
(2) *Initial mound delineation by thresholding:* To find the best parameter for delineating (i.e. isolating) the coral mounds from the rest of the bathymetry data set, several coral mounds were selected as test samples that represent the variation in mound morphologies of the Campeche Mounds. Their basal boundaries were manually outlined with the help of vertically exaggerated 3D-views of the mounds computed in ESRI ArcScene. Within CoMMa, an array of 12 Local Topographic Position derivatives (LTPs), designed to define the elevation of a location (pixel) on a digital elevation model (DEM) relative to its "neighbourhood" (Lindsay et al. 2015; Arosio et al. 2024a, b), with different positioning indices and areal radii (10, 20 and 30 raster pixels) were computed and compared with the manually delineated test samples (see Suppl. mat. V for all LTPs tested). The LTP '*directional median bathymetry positioning index*' (dirM-BPI) with a 30 × 30 pixels radius provided the best fit and was selected for the automatic boundary-based delineation of the coral mounds using a threshold of ≥ 7.5 (BPI ratio units). The dirM-BPI accounts for a sloping neighbourhood (Kim and Wessel 2008) and is therefore well suited for this specific case. As a result, distinct polygon features for all structures, i.e. potential coral mounds, were created.
(3) *Delineation adjustments:* Hebbeln et al. (2012) observed several smaller 'mound' structures of unknown origin that were not formed by corals but may represent contourite drift deposits. Based on this information and in order to provide a conservative estimate of coral mound volume, we excluded topographic features with a height of ≤ 6 m and a feature width of < 71 m. Thin, unusually straight 'mound' structures were identified as multibeam acquisition artefacts and were removed by using a width-length ratio threshold of < 0.12. Ultimately, a 25 m buffer was added to each structure to compensate for the initial vertical cut-off and include the peripheries of the features following Gafeira et al. (2018) and Arosio et al. (2024a). After these adjustments, the final version of the mound polygons was completed.
(4) *Mound volume quantification:* Using the coral mound footprint polygons, two raster data sets were extracted from the initial DEM: raster (i) contains exclusively the coral mound area; raster (ii) contains a hypothetical DEM without mounds that was produced by removing the coral mound areas and closing the produced voids with the Elevation Void Fill Tool in ArcGIS (applying a repetitive inverse distance weighted (IDW) algorithm at 10 pixels resolution). Using the Minus 3D Analyst Tool, we then subtracted raster (ii) from raster (i) and obtained the mound height per pixel. With the produced raster fed into the Surface Volume Tool, the 3D surface area and the total volume of all mound features were determined.

Finally, we multiplied the *total mean carbon concentration* [g C cm^{-3}] with the *total mound volume* [cm^3] to obtain the amount of carbon mass [g C] stored in the Campeche coral mounds, i.e. total carbon storage. As carbon concentrations are first calculated individually for all three carbon fractions, the carbon storage is also obtained for each fraction individually (coral inorganic, sediment inorganic and organic).

Results

Coral ages, mound formation phases and mound aggradation rates

The CWC ages ($n = 53$) obtained from all four on-mound cores range from 1 to 257 kyr BP (27 ages, this study; 26 ages previously published in Matos et al. 2017). Overall, the ages fall into distinct age clusters representing four MFPs (MFP4 to MFP1) separated by hiatuses, i.e. periods without mound formation (sensu Wienberg et al. 2022, see also Suppl. mat. I, III). All on-mound cores collected from the Campeche Mounds show MFP4 (1–10 kyr BP), corresponding to the Holocene. Notably, gravity core GeoB16310-2 over-penetrated when it was retrieved, causing the loss of its top part (Hebbeln et al. 2012). Thus, coral mound formation and aggradation rates could only be reconstructed for the fully recovered part of this core with ages > 5.9 kyr BP. However, a coral fragment recovered from the over-penetrated material shows an age of 0.98 kyr BP, suggesting that mound formation at this coring site equally lasts until today.

Cores GeoB16310-2, GeoB16310-3 and GeoB16318-1 document MFP3 (68–114 kyr BP) roughly corresponding to the ~ MIS5. The two longest cores, GeoB16310-2 and GeoB16310-3, both consistently document a short MFP2 (161–172 kyr BP) during ~ MIS6, while the oldest MFP1 (215–257 kyr BP) corresponding to ~ MIS7/8 is only recovered in core GeoB16310-3 (Fig. 2).

The **MFP4,** corresponding to the Holocene, has the highest vertical mound aggradation rates, ranging from 24 cm kyr^{-1} (GeoB16318-1) to 49 cm kyr^{-1} (GeoB16310-2; see Tables 2, 3). Aggradation rates during the older **MFPs** have significantly lower values of < 11 cm kyr^{-1} (MFP3), ~ 9–12 cm kyr^{-1} (MFP2), and 13 cm kyr^{-1} (MFP1; Tables 2, 3).

Age model and sedimentation rates of the off-mound core

The updated age model of the off-mound core GeoB16320-2 covers a time span of 0–131 kyr BP. Thus, it encompasses the Holocene, last glacial (MIS2-4) and last interglacial (MIS5). In order to make the off-mound results comparable with the on-mound records, we present our data for these three periods based on intervals corresponding to MFP4, the stagnation (hiatus) in mound formation, and MFP3 from the on-mound cores, respectively (Table 4). The herein adjusted ages show only minor differences (< 1 kyr) to the ones originally published by Matos et al. (2017), accordingly, the sedimentation rates (SRs) are also very comparable (for further details on off-mound stratigraphy, see Suppl. mat. IV). SRs vary between 1.5 and 7.2 cm kyr^{-1}, with a total mean of 3.8 cm kyr^{-1}. The mean SRs are slightly higher during the *Holocene* (6 cm kyr^{-1}) and lower during the *last interglacial* (~ MIS 5; 2 cm kyr^{-1}). During the *last glacial*, SRs exhibit a mean of ~ 4 cm kyr^{-1}.

On-mound carbon contents

The CT scans reveal a total mean *coral content* of 7 vol.% (see Suppl. mat. I, III) for the on-mound cores recovered from the Campeche Mounds. When averaged by MFP, the mean coral content values range from 2 to 9 vol.% during MFP4, across the mound records, and were slightly higher during MFP3 (4–14 vol.%). MFP2 has mean coral contents of 8.8–8.9 vol.%, and the record from MFP1 exhibits a mean coral content of 7 vol.%.

The results from the matrix sediment reveal mean *sediment organic carbon contents* ranging from 0.5 to 0.6 wt.% C_{org}, (see Table 3). During MFP3 and MFP2, C_{org} contents decrease down to mean ranges between 0.2 and 0.3 wt.%, respectively. MFP1, documented in GeoB16310-3 from Ixchel Mound, has a sediment C_{org} content of 0.4 wt.%. The mean *sediment inorganic carbon contents*, remain relatively constant throughout the cores and MFPs, with no major trends ranging between 9.7 and 10.5 wt.% C_{inorg} in total. Notably, the presented $C_{inorg.}$ values convert to mean sediment carbonate contents between 81 and 87 wt.% $CaCO_3$ on the mounds.

Altogether, the three carbon fractions exhibit a total mean *carbon concentration* of 0.11 g C cm^{-3} (± 0.018 SD) across all data points from the mound records. Across the specific mound formation phases (Table 3), the carbon concentration stays rather constant, between 0.10 and 0.11 g C cm^{-3} during MFP4, 0.11–0.14 g C cm^{-3} during MFP3, 0.12–0.14 g C cm^{-3} during MFP2 and around 0.12 g C cm^{-3} during MFP1.

On-mound carbon accumulation rates

Total carbon accumulation on the coral mounds ranges from 0.5 to 5.6 g C cm^{-2} kyr^{-1} (see Table 3, Fig. 3). This can be subdivided into 0.1–1.3 g C cm^{-2} kyr^{-1} *coral* C_{inorg}, 0.4–4.0 g C cm^{-2} kyr^{-1} *sed.* C_{inorg} and 0.01–0.2 g C cm^{-2} kyr^{-1} *sed.* C_{org}. All mound records have a similar overall trend throughout their history, with higher rates of carbon accumulation during MFP4, and lower rates during

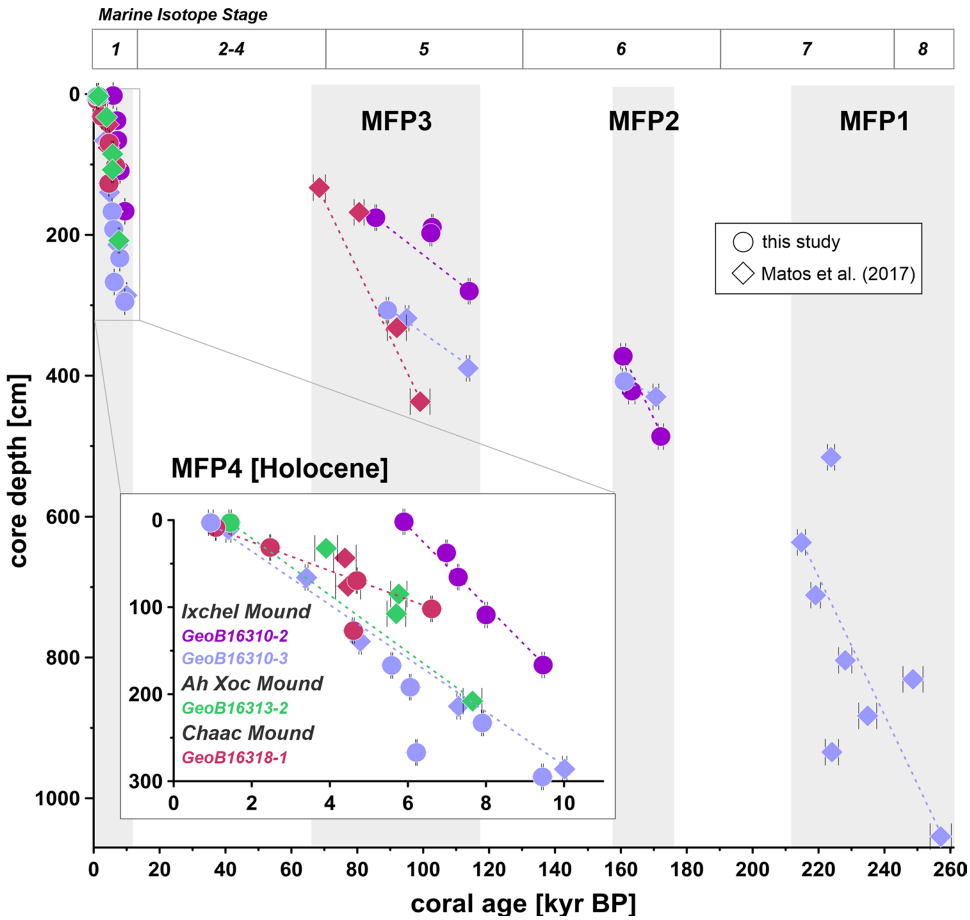

Fig. 2 ^{230}Th/U coral ages obtained from four on-mound cores (see colour code for differentiation) collected in the Campeche Mound Province. Data are shown as age vs. core depth profile (circles: this study ($n=26$); diamonds: previously published in Matos et al. 2017 ($n=26$), see Table 2 for details. The coral age from the over-penetrated part of GeoB16310-2 is excluded from this figure, as it cannot be assigned to a core depth. Black bars bordering each age data point indicate the age error. Coral ages from cores GeoB16310-2 and GeoB16310-3 (Ixchel Mound) are given in purple/light blue, from core GeoB16313-2 (Ah Xoc Mound) in green, and from core GeoB16318-1 (Chaac Mound) in red. Mound formation phases (MFP1–MFP4) indicated by distinct age clusters are marked by grey vertical boxes. Marine isotope stages (MISs) corresponding to the timeline are indicated in the top box. Due to the large number of coral ages from the MFP4 corresponding to the Holocene, a zoom-in (bottom left) is provided for more detail using the same axis units

MFP3 and earlier (Fig. 3, Table 3). During MFP4, mean values range from 2.4 to 5.6 g C cm^{-2} kyr^{-1}. During MFP3, the mean carbon accumulation rate was lower, with a range of 0.5–1.2 g C cm^{-2} kyr^{-1}. During MFP2, the mean carbon accumulation was documented at 1.3–1.5 g C cm^{-2} kyr^{-1} from the two cores on Ixchel Mound (GeoB16310-2 and GeoB16310-3). Finally, during MFP1, mean carbon accumulation amounts to 1.6 g C cm^{-2} kyr^{-1} on Ixchel Mound (GeoB16310-3). Notably, the mean carbonate accumulation (based on total C_{inorg} rates) ranges from 4 to 44 g $CaCO_3$ cm^{-2} kyr^{-1} throughout the MFPs, following the same general trends as for the carbon accumulation (Table 3). Irrespective of the time and location, the sediment C_{inorg} fraction contributes the majority of carbon to the carbon accumulation, followed by coral-derived carbon, and to a minor degree, C_{org}. Overall, C_{org} has a contribution to the total on-mound carbon accumulation of 2–5%, while the sediment C_{inorg} fraction contributes with 72–88%, and the coral C_{inorg} fraction accounts for an additional 7–24% (Fig. 3).

Off-mound carbon contents and accumulation rates

The Holocene carbon content in the off-mound record (Table 4) exhibits a mean C_{org} content of 0.5 wt.% (±0.1 SD), and a C_{inorg} content of 10.4 wt.% (±0.2 SD) and does not vary substantially between the last glacial and interglacial. During the last interglacial, mean C_{org} content is 0.3 wt.% (<0.1 SD), and C_{inorg} content 10.3 wt.% (±0.9 SD). During the glacial, the mean C_{org} content lies at 0.3 wt.%, and C_{inorg} at 10.5 wt.%. This corresponds to a variation in mean carbonate content of 86–88 wt.%. The total mean carbon concentration of the off-mound record is

Table 2 ^{230}Th/U cold-water coral ages obtained from four on-mound cores collected in the Campeche Mound Province

core ID [GeoB]	core depth [cm]	species	Labcode	δ^{234}U(i) [‰]	±	^{232}Th [ng/g]	±	Age [kyr BP]	±	MFP	AR [cm kyr^{-1}]	Source
16310–2*	**0**	***Lp***	**IUP-12616**	**147.5**	**0.4**	**0.1245**	**0.0007**	**0.905**	**0.007**	**4**	**49**	**This study**
16310–2	**2**	***Lp***	**IUP-12297**	**146.3**	**0.5**	**0.2971**	**0.0009**	**5.898**	**0.025**	**4**		**This study**
16310–2	**38**	***Lp***	**IUP-12193**	**146.3**	**0.4**	**0.1451**	**0.0003**	**6.987**	**0.019**	**4**		**This study**
16310–2	**66**	***Lp***	**IUP-12194**	**145.5**	**0.4**	**0.3295**	**0.0005**	**7.289**	**0.018**	**4**		**This study**
16310–2	**109**	***Lp***	**IUP-12163**	**146.7**	**0.6**	**0.1781**	**0.0006**	**8.003**	**0.035**	**4**		**This study**
16310–2	**167**	***Lp***	**IUP-12164**	**145.6**	**0.7**	**0.5012**	**0.0011**	**9.465**	**0.036**	**4**		**This study**
16310–2	**176**	***Lp***	**IUP-12165**	**145.7**	**1.1**	**0.7784**	**0.0015**	**85.601**	**0.251**	**3**	**6**	**This study**
16310–2	**189**	***Lp***	**IUP-12166**	**145.1**	**0.6**	**0.6892**	**0.0013**	**102.750**	**0.251**	**3**		**This study**
16310–2	**198**	***Lp***	**IUP-12167**	**146.7**	**0.7**	**0.2940**	**0.0007**	**102.325**	**0.299**	**3**		**This study**
16310–2	**280**	***Lp***	**IUP-12168**	**147.6**	**0.6**	**0.3246**	**0.0005**	**113.962**	**0.301**	**3**		**This study**
16310–2	**373**	***Lp***	**IUP-12169**	**142.8**	**0.8**	**0.7906**	**0.0021**	**160.668**	**0.758**	**2**	**12**	**This study**
16310–2	**422**	***Lp***	**IUP-12170**	**142.6**	**1.2**	**0.2983**	**0.0008**	**163.302**	**0.974**	**2**		**This study**
16310–2	**487**	***Lp***	**IUP-12195**	**140.8**	**0.7**	**0.6318**	**0.0012**	**172.125**	**0.805**	**2**		**This study**
16310–3	**3**	***Lp***	**IUP-12290**	**147.8**	**0.5**	**2.4114**	**0.0066**	**0.952**	**0.062**	**4**	**34**	**This study**
16310–3	11	*Lp*	GIF-3370	147.4	1.1	0.8371	0.0007	1.403	0.063	**4**		Matos et al. (2017)
16310–3	66	*Ep*	GIF-3371	146.1	1.3	0.3709	0.0005	3.404	0.038	**4**		Matos et al. (2017)
16310–3	140	*Lp*	GIF-3416	147.3	2.2	0.1912	0.0003	4.778	0.032	**4**		Matos et al. (2017)
16310–3	**167**	***Lp***	**IUP-12291**	**146.6**	**0.7**	**0.1664**	**0.0006**	**5.586**	**0.022**	**4**		**This study**
16310–3	**192**	***Lp***	**IUP-12292**	**146.2**	**0.5**	**0.1116**	**0.0004**	**6.060**	**0.020**	**4**		**This study**
16310–3	214	*Ep*	GIF-3417	144.7	1.5	0.4516	0.0003	7.296	0.044	**4**		Matos et al. (2017)
16310–3	**233**	***Lp***	**IUP-12293**	**146.3**	**0.4**	**0.3088**	**0.0006**	**7.908**	**0.024**	**4**		**This study**
16310–3	**267**	***Lp***	**IUP-12294**	**146.0**	**0.5**	**0.1017**	**0.0003**	**6.216**	**0.019**	**4**		**This study**
16310–3	286	*Lp*	GIF-3418	149.4	1.3	0.3296	0.0005	10.015	0.057	**4**		Matos et al. (2017)
16310–3	**295**	***Lp***	**IUP-12295**	**145.3**	**0.5**	**0.3407**	**0.0007**	**9.445**	**0.024**	**4**		**This study**
16310–3	**307**	***Lp***	**IUP-12296**	**144.3**	**0.8**	**1.0667**	**0.0025**	**89.137**	**0.370**	**3**	**4**	**This study**
16310–3	319	*Lp*	GIF-3420	144.5	2.3	1.4276	0.0008	95.098	0.570	**3**		Matos et al. (2017)
16310–3	390	*Lp*	GIF-3421	143.6	2.2	0.3230	0.0007	113.626	0.534	**3**		Matos et al. (2017)
16310–3	**408**	***Lp***	**IUP-13478**	**141.7**	**0.8**	**0.5939**	**0.0009**	**161.038**	**0.535**	**2**	**9**	**This study**
16310–3	430	*Lp*	GIF-3422	151.7	2.1	0.6894	0.0005	170.631	0.888	**2**		Matos et al. (2017)
16310–3	516	*Lp*	GIF-3423	152.2	1.8	0.2267	0.0003	223.800	1.087	**1**	**13**	Matos et al. (2017)
16310–3	637	*Lp*	GIF-3424	141.8	2.1	0.2512	0.0002	214.783	1.208	**1**		Matos et al. (2017)
16310–3	712	*Lp*	GIF-3426	147.6	2.1	0.2122	0.0004	219.116	1.466	**1**		Matos et al. (2017)
16310–3	804	*Lp*	GIF-3427	149.2	3.3	0.2979	0.0003	228.087	1.997	**1**		Matos et al. (2017)
16310–3	831	*Lp*	GIF-3398	153.6	3.1	0.6433	0.0009	248.647	3.043	**1**		Matos et al. (2017)
16310–3	883	*Lp*	GIF-3399	152.2	4.2	0.6326	0.0007	234.898	2.731	**1**		Matos et al. (2017)
16,310–3	935	*Lp*	GIF-3400	146.7	3.2	0.1688	0.0006	224.036	2.031	**1**		Matos et al. (2017)
16,310–3	1055	*Lp*	GIF-3401	156.1	4.1	0.3731	0.0006	257.070	3.215	**1**		Matos et al. (2017)

Table 2 (continued)

core ID [GeoB]	core depth [cm]	species	Labcode	$\delta^{234}U(i)$ [‰]	±	^{232}Th [ng/g]	±	Age [kyr BP]	±	MFP	AR [cm kyr^{-1}]	Source
16,313–2	**3**	***Lp***	**IUP-13476**	**147.7**	**1.3**	**0.7648**	**0.0033**	**1.446**	**0.030**	**4**	**40**	**This study**
16,313–2	33	*Lp*	IUP-6795	151.1	4.0	0.1065	0.0100	3.905	0.290	**4**		Matos et al. (2017)
16,313–2	85	*Lp*	IUP-6796	150.5	4.4	0.1356	0.0100	5.765	0.210	**4**		Matos et al. (2017)
16,313–2	108	*Lp*	IUP-6797	148.1	3.7	0.4468	0.0150	5.705	0.240	**4**		Matos et al. (2017)
16,313–2	208	*Lp*	IUP-6798	147.5	3.6	0.4030	0.0160	7.655	0.240	**4**		Matos et al. (2017)
16,318–1	**9**	***Lp***	**IUP-12196**	**146.6**	**0.4**	**0.1476**	**0.0003**	**1.078**	**0.008**	**4**	**24**	**This study**
16,318–1	**32**	***Ep***	**IUP-12197**	**144.7**	**0.4**	**0.4024**	**0.0008**	**2.472**	**0.013**	**4**		**This study**
16,318–1	44	*Lp*	IUP-6788	149.4	3.0	0.5566	0.0070	4.385	0.290	**4**		Matos et al. (2017)
16,318–1	**70**	***Lp***	**IUP-12198**	**146.6**	**0.4**	**0.3199**	**0.0005**	**4.691**	**0.014**	**4**		**This study**
16,318–1	76	*Lp*	IUP-6789	149.6	3.9	0.1213	0.0030	4.465	0.320	**4**		Matos et al. (2017)
16,318–1	**102**	***Ep***	**IUP-12199**	**145.9**	**0.4**	**0.3387**	**0.0007**	**6.608**	**0.021**	**4**		**This study**
16,318–1	**127**	***Lp***	**IUP-12200**	**145.9**	**0.6**	**0.3637**	**0.0008**	**4.605**	**0.024**	**4**		**This study**
16,318–1	133	*Lp*	IUP-6790	155.9	5.8	0.5030	0.0100	68.495	1.850	**3**	**11**	Matos et al. (2017)
16,318–1	168	*Lp*	IUP-6791	146.2	4.2	0.3320	0.0080	80.545	1.510	**3**		Matos et al. (2017)
16,318–1	332	*Lp*	IUP-6793	145.0	3.9	1.8067	0.0270	92.005	2.880	**3**		Matos et al. (2017)
16,318–1	437	*Lp*	IUP-6794	147.5	5.3	0.2551	0.0120	99.055	3.000	**3**		Matos et al. (2017)

Provided are decay corrected $^{234}U/^{238}U$ activity ratios ($\delta^{234}U(i)$) and ^{232}Th concentrations. Coral ages ($n = 27$) newly obtained for this study are indicated in bold, ages previously published by Matos et al. (2017; $n = 26$) are given in regular. Coral species *Lophelia pertusa* and *Enallopsammia profunda* are indicated as "Lp" and "Ep", respectively. Mound formation phases (MFP) correspond to the Holocene (MFP4), ~MIS5 (MFP3), ~MIS6 (MFP2), and ~MIS7/8 (MPF1). (*) discarded for age model, since relative depth unknown due to material loss between this and second age

0.11 g C cm^{-3} (±0.01 SD), which remains relatively constant with a mean of 0.10 (<0.01 SD) for the Holocene, and 0.11 (±0.01 SD) g C cm^{-3} for both last glacial and interglacial. Irrespective of the time and location, the C_{inorg} fraction contributes the majority of carbon to the mean off-mound carbon accumulation, with 96–97%, while the C_{org} contributes 3–4% throughout. The mean total carbon accumulation in the off-mound record during the Holocene (corresponding to MFP4, 01–10 kyr BP) is 0.57 g C cm^{-2} kyr^{-1} (±0.11 SD), which can be subdivided into 0.55 g C_{inorg} cm^{-2} kyr^{-1} and 0.03 g C_{org} cm^{-2} kyr^{-1} (note that the observed mismatch arises from decimal rounding). During the glacial (stagnation of mound formation between MFP4 and MFP3; 11–68 kyr BP), we find a mean carbon accumulation rate of 0.47 g C cm^{-2} kyr^{-1} (±0.2 SD), consisting of 0.46 g C_{inorg} cm^{-2} kyr^{-1} and 0.01 g C_{org} cm^{-2} kyr^{-1}. The mean off-mound carbon accumulation during the last interglacial (analogous to the on-mound record for MFP3, 68–114 kyr BP) is about half of that with 0.23 g C cm^{-2} kyr^{-1} (±0.06 SD), consisting of 0.22 g C_{inorg} cm^{-2} kyr^{-1} and 0.01 g C_{org} cm^{-2} kyr^{-1}.

Estimation of carbon storage in the Campeche mounds

The mound delineation (Fig. 4) through CoMMa revealed interconnected mounds in the shape of elongated ridges with several peaks that can be > 2.5 km long and can cover an area of > 0.5 km^2 per coral mound ridge. The Campeche Mounds are estimated to have an areal coverage of 16.7 km^2 (corresponding to a 3D surface area of the CWC reef habitat area of 17.7 km^2), which is about ~12% of the entire mapped area. For the 145 mound ridges, we identified a total mound volume of 0.162 km^3 for the entire mapped area of the Campeche Mound Province. Combining the mean total carbon concentration of 0.11 g C cm^{-3} (±0.01 SD; 0.02 g C cm^{-3} coral C_{inorg}; 0.09 g C cm^{-3} sed. C_{inorg}; and <0.01 g C cm^{-3} sed. C_{org}) of all data points from the mound records with the mound volume, the carbon stored in the Campeche Mounds is estimated to be 18.5 megatons [Mt] carbon (±2.9 SD, based on the variation in mound carbon concentration). With a mean share of 3.3% C_{org} in total carbon concentration, this leads to an organic carbon storage of 0.6 Mt C_{org} (±0.1 SD). The coral C_{inorg} contributes up to 15.6% equalling 2.9 Mt C_{inorg} (±0.5 SD), and the sediment C_{inorg} contributes 81.1% equalling 15.0 Mt C_{inorg} (±2.4 SD).

Discussion

Carbon accumulation patterns of the Campeche Mounds

The carbon accumulation of the Campeche Mounds is steered by mound aggradation, consistent with previous observations showing a general significant correlation between aggradation rates and carbonate accumulation rates for coral mounds in the Mediterranean Sea and off Norway (e.g. Greiffenhagen et al. 2025a; Titschack et al. 2015; 2016). Aggradation rates for the Campeche Mounds of 4–49 cm kyr^{-1} (Table 3) correspond to carbon accumulation rates of 0.5–5.6 g C_{total} cm^{-2} kyr^{-1}, which are low to moderate (according to the definition proposed by Greiffenhagen et al. 2025a; *low < ~2 > moderate < ~12 g* C_{total} *cm^{-2} kyr^{-1} < enhanced*). Enhanced carbon accumulation rates of up to 15 g C_{total} cm^{-2} kyr^{-1} have been reported for individual coral mounds in the western Mediterranean Sea (Greiffenhagen et al. 2025a), i.e. almost three times higher than those of the Campeche Mounds. Reports from other regions so far only consider inorganic carbon accumulation rates, thereby neglecting the contribution of organic carbon. Such inorganic carbon accumulation rates for coral mounds range from enhanced (> 12 g C_{inorg} cm^{-2} kyr^{-1}; Norwegian shelf, Titschack et al. 2015) to moderate (up to ~7 g C_{inorg} cm^{-2} kyr^{-1}; eastern Mediterranean Sea, Titschack et al. 2016) and to low rates (< ~2 g C_{inorg} cm^{-2} kyr^{-1}; off Ireland, Dorschel et al. 2007; Titschack et al. 2009; and in the Bay of Biscay, Edinger et al. 2025).

Considering average sediment contents in coral mounds are > 75% (e.g. Titschack et al. 2015; Corbera et al. 2021), and the important role of external sediment supply in fuelling overall mound aggradation (Wang et al. 2021), it is apparent that mound carbon accumulation is closely tied to ambient sedimentation rates. Correspondingly, in the Campeche Mound Province, not only the mound carbon accumulation, but also the mean off-mound sedimentation rates are about three times lower (4–6 cm kyr^{-1}) than in the off-mound record of the East Melilla Mound Province (12–16 cm kyr^{-1} SR; Greiffenhagen et al. 2025a). The low to moderate aggradation rates and subsequent carbon accumulation rates of the Campeche Mounds are most likely not related to sub-optimal conditions for CWC growth, but are the consequence of limited sediment availability in the area (Matos et al. 2017). The study area of the Campeche Bank margin receives low sediment supply as there are no large rivers or dust sources (i.e. deserts) in the hinterland (Domínguez-Castanedo et al. 2012) that could deliver terrigenous, siliciclastic material.

Conspicuous for the Campeche Mounds is a low mean coral content with ~7 vol.%, which is about half or even less of that reported for other mound provinces (e.g. 14–23 vol.%; Norway or Alborán Sea; Titschack et al. 2015; Corbera et al. 2021), further underlining the key role of sediment supply. In fact, the Campeche Mounds are remarkable in that they are dominated by carbonate sediments, unlike most other coral mound provinces which are dominated by siliciclastic sediments: They exhibit the highest mean carbonate contents (81–87 wt.%) measured

Table 3 All on-mound carbon(ate) accumulation rate and content data from this study per mound formation phase (MFP)

Mound formation phase (MFP)	AR/SR [cm kyr^{-1}]	C_{org} [wt.%]	C_{inorg} [wt.%]	Total C Conc. [g C cm^{-3}]	Sediment C_{org} Acc. [g C_{org} cm^{-2} kyr^{-1}]	Sediment C_{inorg} Acc. [g C_{inorg} cm^{-2} kyr^{-1}]	Coral C_{inorg} Acc. [g C_{inorg} cm^{-2} kyr^{-1}]	Total Carbonate Acc. [g $CaCO_3$ cm^{-2} kyr^{-1}]	Total C Acc [g C cm^{-2} kyr^{-1}]
MFP4, HOLOCENE (0–10 kyr BP)									
GeoB16310-2	**49**	**0.61** ± 0.07	**10.23** ± 0.09	**0.11** ± 0.008	**0.24** ± 0.019	**4.01** ± 0.34	**1.31** ± 0.50	**44** ± 3.23	**5.56** ± 0.37
GeoB16310-3	**34**	**0.61** ± 0.07	**10.24** ± 0.18	**0.10** ± 0.008	**0.16** ± 0.020	**2.72** ± 0.33	**0.40** ± 0.20	**26** ± 2.32	**3.28** ± 0.28
GeoB16313-2	**40**	**0.58** ± 0.08	**10.35** ± 0.10	**0.11** ± 0.005	**0.19** ± 0.023	**3.40** ± 0.13	**0.82** ± 0.23	**35** ± 1.81	**4.41** ± 0.20
GeoB16318-1	**24**	**0.53** ± 0.10	**10.46** ± 0.16	**0.10** ± 0.011	**0.10** ± 0.010	**2.14** ± 0.32	**0.18** ± 0.10	**19** ± 2.22	**2.43** ± 0.26
Off-mound mean	*6*	*0.49 ± 0.09*	*10.35 ± 0.19*	*0.10 ± 0.004*	*0.03 ± 0.006*	*0.56 ± 0.08*	*n/a*	*5 ± 0.63*	*0.58 ± 0.08*
MFP3, ~MIS5 (68–114 kyr BP)									
GeoB16310-2	**6**	**0.27** ± 0.12	**10.41** ± 0.19	**0.13** ± 0.009	**0.02** ± 0.007	**0.61** ± 0.03	**0.19** ± 0.05	**7** ± 0.41	**0.82** ± 0.05
GeoB16310-3	**4**	**0.29** ± 0.13	**10.43** ± 0.11	**0.14** ± 0.006	**0.01** ± 0.005	**0.42** ± 0.03	**0.11** ± 0.04	**4** ± 0.22	**0.54** ± 0.02
GeoB16318-1	**10**	**0.32** ± 0.09	**9.74** ± 1.70	**0.11** ± 0.021	**0.03** ± 0.010	**1.00** ± 0.20	**0.16** ± 0.11	**10** ± 1.87	**1.19** ± 0.23
Off-mound mean	*2*	*0.29 ± 0.03*	*10.40 ± 0.48*	*0.11 ± 0.007*	*0.01 ± 0.002*	*0.21 ± 0.05*	*n/a*	*2 ± 0.45*	*0.22 ± 0.06*
MFP2, ~MIS6 (161–172 kyr BP)									
GeoB16310-2	**12**	**0.26** ± 0.02	**10.19** ± 0.23	**0.12** ± 0.004	**0.03** ± 0.004	**1.30** ± 0.04	**0.15** ± 0.09	**12** ± 0.42	**1.49** ± 0.05
GeoB16310-3	**9**	**0.22** ± 0.001	**10.48** ± 0.001	**0.14** ± 0.002	**0.02** ± 0.001	**1.01** ± 0.03	**0.26** ± 0.01	**11** ± 0.12	**1.29** ± 0.01
MFP1, ~MIS7/8 (215–257 kyr BP)									
GeoB16310-3	**13**	**0.41** ± 0.07	**10.44** ± 0.20	**0.12** ± 0.006	**0.05** ± 0.008	**1.32** ± 0.09	**0.24** ± 0.11	**13** ± 0.68	**1.61** ± 0.08

Values per MFP are shown for each corresponding core record. For comparison, the off-mound core GeoB16320-2 is shown in italics (mean of all time equal comparisons with the on-mound cores, see Fig. 3). Data presented include mound aggradation rates (AR; for off-mound core: SR as sedimentation rates), organic and inorganic carbon content of the sediment (C_{org}/C_{inorg}), the total carbon mass concentration (Total C Conc.), all fractions of carbon accumulation (Acc.) with their rates, as well as the total carbonate ($CaCO_3$; derived from C_{inorg}) accumulation and the total carbon accumulation rate. Means are given in bold, ± standard deviation in light

Table 4 All data related to carbon(ate) accumulation rates in the off-mound core GeoB16320-2, including sedimentation rate (SR), organic and inorganic carbon contents (C_{org}/C_{inorg}), the total carbon mass concentration (Total C Conc.), all fractions of carbon accumulation (C Acc.) with their rates, as well as the total carbonate (derived from C_{inorg} Acc.) and the total C Acc rates

core depth [m]	Age [kyr BP]	SR [cm kyr^{-1}]	C_{org} content [wt.%]	C_{inorg} content [wt.%]	Total C Conc. [g C cm^{-3}]	C_{org} Acc. [g C_{org} cm^{-2} kyr^{-1}]	C_{inorg} Acc. [g C_{inorg} cm^{-2} kyr^{-1}]	Carbonate Acc. [g $CaCO_3$ cm^{-2} kyr^{-1}]	Total C Acc. [g C_{total} cm^{-2} kyr^{-1}]
0.03	**1.94**	**6.1**	**0.68**	**9.92**	**0.09**	**0.04**	**0.54**	**4.47**	**0.57**
0.08	**2.69**	**5.8**	**0.60**	**10.10**	**0.10**	**0.03**	**0.53**	**4.38**	**0.56**
0.13	**3.56**	**5.3**	**0.62**	**10.18**	**0.10**	**0.03**	**0.49**	**4.10**	**0.52**
0.18	**4.50**	**4.5**	**0.44**	**10.36**	**0.10**	**0.02**	**0.43**	**3.61**	**0.45**
0.23	**5.60**	**6.1**	**0.41**	**10.39**	**0.10**	**0.02**	**0.59**	**4.89**	**0.61**
0.28	**6.42**	**5.5**	**0.41**	**10.50**	**0.10**	**0.02**	**0.55**	**4.57**	**0.57**
0.33	**7.44**	**6.7**	**0.44**	**10.56**	**0.11**	**0.03**	**0.67**	**5.62**	**0.70**
0.38	**8.26**	**6.1**	**0.44**	**10.56**	**0.11**	**0.03**	**0.62**	**5.15**	**0.64**
0.43	**9.12**	**7.0**	**0.41**	**10.39**	**0.10**	**0.03**	**0.71**	**5.92**	**0.74**
0.48	**9.83**	**3.3**	**0.41**	**10.70**	**0.11**	**0.01**	**0.35**	**2.88**	**0.36**
0.53	11.14	4.8	0.40	10.80	0.11	0.02	0.51	4.29	0.53
0.68	14.44	4.5	0.38	10.43	0.11	0.02	0.47	3.92	0.49
0.98	20.08	7.2	0.33	10.87	0.12	0.03	0.88	7.32	0.90
1.28	25.02	4.2	0.35	10.85	0.11	0.02	0.47	3.94	0.49
1.58	32.87	3.8	0.28	10.23	0.12	0.01	0.45	3.76	0.46
1.88	40.14	3.4	0.33	10.47	0.12	0.01	0.39	3.23	0.40
2.18	50.70	2.9	0.23	10.27	0.11	0.01	0.32	2.63	0.32
2.48	65.43	1.7	0.29	10.21	0.11	0.01	0.19	1.56	0.19
2.78	**77.71**	**3.0**	**0.26**	**7.55**	**0.08**	**0.01**	**0.23**	**1.96**	**0.24**
3.08	**88.18**	**3.0**	**0.28**	**10.42**	**0.11**	**0.01**	**0.33**	**2.75**	**0.34**
3.13	**89.91**	**1.5**	**0.25**	**10.55**	**0.12**	**0.00**	**0.17**	**1.43**	**0.18**
3.18	**92.74**	**1.8**	**0.30**	**10.50**	**0.12**	**0.01**	**0.20**	**1.65**	**0.20**
3.23	**95.69**	**1.6**	**0.31**	**10.60**	**0.12**	**0.01**	**0.18**	**1.52**	**0.19**
3.28	**98.59**	**1.7**	**0.28**	**10.62**	**0.12**	**0.01**	**0.20**	**1.63**	**0.20**
3.33	**101.37**	**1.6**	**0.27**	**10.63**	**0.12**	**0.00**	**0.19**	**1.58**	**0.19**
3.38	**104.41**	**1.9**	**0.28**	**10.82**	**0.12**	**0.01**	**0.23**	**1.89**	**0.23**
3.43	**107.14**	**1.6**	**0.29**	**10.51**	**0.12**	**0.00**	**0.18**	**1.50**	**0.18**
3.48	**110.26**	**1.7**	**0.36**	**10.44**	**0.11**	**0.01**	**0.19**	**1.60**	**0.20**
3.53	**113.13**	**2.9**	**0.36**	**10.64**	**0.11**	**0.01**	**0.32**	**2.69**	**0.33**
3.58	114.72	2.5	0.33	10.37	0.11	0.01	0.26	2.17	0.27
3.63	116.44	3.5	0.31	10.59	0.11	0.01	0.37	3.08	0.38
3.68	118.05	2.9	0.29	10.51	0.11	0.01	0.31	2.55	0.31
3.98	127.98	3.6	0.25	10.95	0.13	0.01	0.45	3.75	0.46

Values that correspond to mound formation phases (MFP4 and MFP3) are presented in bold, with the glacial (hiatus/stagnation of mound formation between MFP4 and MFP3) in between, and some earlier values before MFP3 (> 114 kyr BP)

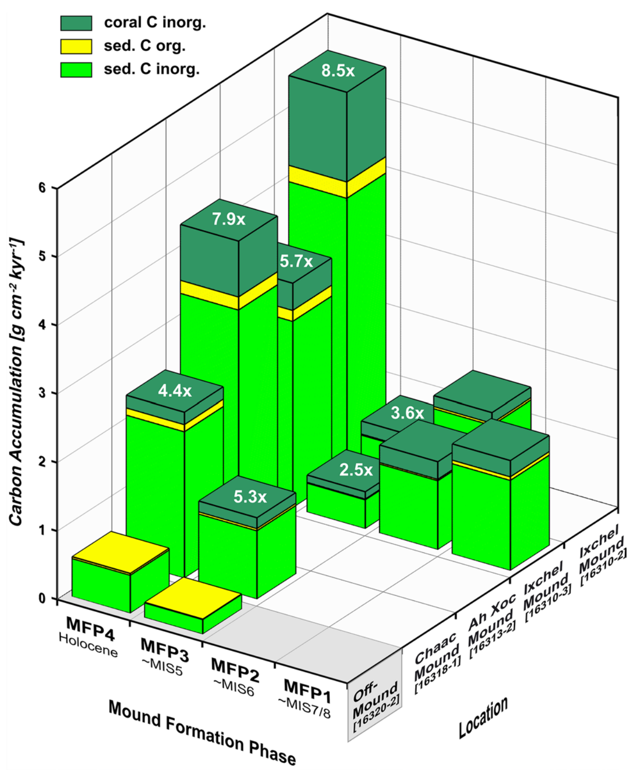

Fig. 3 Spatio-temporal presentation of carbon accumulation (in g C cm^{-2} kyr^{-1}; y-axis) in the Campeche Mound Province from ~ 257 kyr BP until present encompassing four mound formation phases (MFP4 to MFP1, x-axis; from present till the oldest record; note that the axis is not to scale, but divided into nominal time periods). The carbon accumulation (shown as stacked bars) is subdivided into the three carbon fractions: sediment organic carbon (yellow), sediment inorganic carbon (C_{inorg}; light green), and coral C_{inorg} (dark green, only relevant for on-mound cores). Spatially, the results are shown per location and GeoB core ID labels along the z-axis. The off-mound record is shown in grey. White numbers on the bars indicate the factor by how many times the total on-mound carbon accumulation exceeds the off-mound accumulation, during the same time period (mound-specific MFP durations considered). Since the off-mound carbon accumulation record does not date back further than ~ 128 kyr, an on-/off-mound comparison is not possible for the two oldest MFPs 1 and 2

for coral mounds so far (< 55 wt.% for coral mounds in the NE and NW Atlantic and Mediterranean Sea, see Kiriakoulakis et al. 2007; Dorschel et al. 2007; Mienis et al. 2009; Matos et al. 2015; Titschack et al. 2009, 2015, 2016; Greiffenhagen et al. 2025a; Edinger et al. 2025). This appears logical as the Campeche Mound Province is connected to the Campeche Bank carbonate shelf, which is fully dominated by calcareous sediments (Craeger 1959; Holmes 1976; Balsam and Beeson 2003). Notably, the large proportion of sedimentary inorganic carbon (in both on- and off-mound records), and the proximity to the Campeche carbonate shelf suggest that, initially, much of the carbon buried in the mounds was produced by the pelagic carbonate factory. However, ultimately, its rapid burial was triggered by the coral factory through the baffling capacity of the coral frameworks on the mound. This triggering effect of carbon burial is emphasised by the surplus of carbon accumulated in the mound records (see Fig. 3; compared to the off-mound), representing the carbon burial due solely to the ecosystem engineering of CWCs.

The age models of all our mound records show roughly consistent trends of MFPs timings (see Fig. 2). This demonstrates that mound formation takes place almost synchronously across the Campeche Mounds. MFP-specific mean carbon accumulation rates (during the same period) are relatively consistent, which is indicated by smaller value ranges within MFPs compared to the overall range of 0.5–5.6 g C_{total} cm^{-2} kyr^{-1} (Table 3). For example, the Holocene carbon accumulation rates from MFP4, with values ranging from 2.4 to 5.6 g C_{total} cm^{-2} kyr^{-1}, are consistently ≥ 2 times higher than those from MFP3, with values ranging from 0.8 to 1.2 g C_{total} cm^{-2} kyr^{-1}.

The intra-mound variation in carbon accumulation (within one mound) lies in the range of the inter-mound variation (between mounds) at any given period, for example, during MFP4, 3.3–5.6 g C_{total} cm^{-2} kyr^{-1} on Ixchel Mound; 2.4–5.6 g C_{total} cm^{-2} kyr^{-1} on all mounds. Hence, we suggest that the variation in carbon accumulation is rather a function of intra-mound aggradation patterns, i.e. variations of reef growth across an individual mound, than changes in carbon accumulation between individual mounds (inter-mound variability). Although there is still some variation in carbon accumulation rates in the Campeche Mounds, these are rather consistent in comparison to other mound provinces, where diachronous mound formation occurs amongst nearby mounds (i.e. Alborán Sea; Wienberg et al. 2022; Corbera et al. 2021), and also wider ranges of MFP-specific aggradation rates can be found (e.g. off Mauritania; Wienberg et al. 2018). In summary, the relative synchroneity and consistency in carbon accumulation between the studied mound records suggest that they are representative of all coral mounds in the Campeche Mound Province and can be used for upscaling.

Comparing on- and off-mound carbon accumulation in the Campeche Mound Province

For the area of the Campeche Escarpment, Hübscher & Nürnberg (2023) present sedimentation rates of ~ 3.5 cm kyr^{-1} for the last ~ 130 kyr, which is close to the mean sedimentation rate of 3.1 cm kyr^{-1} in our off-mound record over the same time period. A comprehensive study on carbonate accumulation in the region found average rates of 0.2–0.3 g C_{inorg} cm^{-2} kyr^{-1}, which are very comparable to our overall mean off-mound inorganic carbon accumulation of ~ 0.4 g $C_{inorg.}$ cm^{-2} kyr^{-1}, and similarly high carbonate

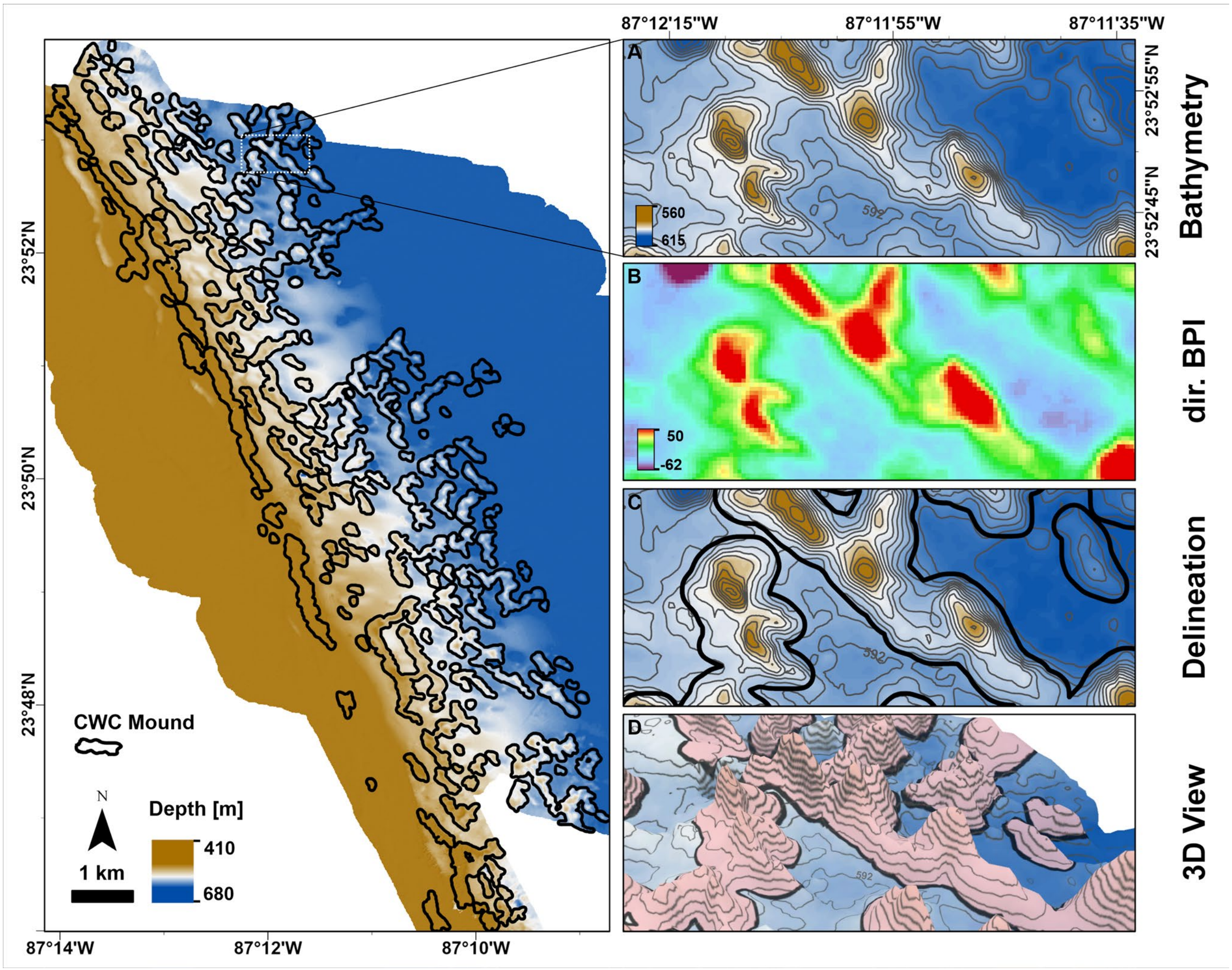

Fig. 4 Result of the CoMMa Toolbox-based delineation of the Campeche cold-water coral (CWC) mounds from bathymetry, as the basis for the total mound volume calculation. Left: Main map showing the overall result with outline/footprint of coral mounds (black) in the Campeche Mound Province on top of the bathymetry map of the area (see Fig. 1). Right: Step-by-step illustration of the CoMMa-based mound delineation, using an excerpt as an example (white-dotted box in left map). **a** Bathymetry (symbology following dynamic range adjustment), including 4 m-contour lines. **b** the chosen local topographic position derivative metrics of the exact same location (directional Median of BPI; dir. BPI, 30×30 pixels neighbourhood, see step 2 in methods), **c** the subsequent, threshold-based delineation of the mounds (≥7.5 cut-off, minimum width, relief height and width-length ratio adjusted, see step 3 in methods). **d** the same outline (area in light red; 6×vertical exaggeration) in 3D view perspective (indicating the volume obtained)

contents at a slightly deeper site near the Campeche Mound Province (Díaz-Ascencio et al. 2023; see also Schönfeld 2010). Thus, we suggest that the off-mound core used in this study is also representative of the area and can confidently be compared with the on-mound accumulation rates.

In order to evaluate the effectiveness of carbon accumulation in any ecosystem, it is important to consider the rate of total carbon accumulation in relation to the surrounding environment (off-mound; background rate). The overall carbon accumulation for the Campeche Mounds is estimated to be 0.5–5.6 g C_{total} cm^{-2} kyr^{-1} during phases of active mound formation, whilst in the off-mound, 0.2–0.6 g C_{total} cm^{-2} kyr^{-1} are accumulated. The overall surplus carbon accumulation rate, defined as coral mound carbon accumulation rate *minus* background rate, ranges from 0.3 to 4.9 g C cm^{-2} kyr^{-1} for all records.

In more detail, differences in carbon accumulation between the Campeche Mounds and the surrounding environment can be presented through calculating the ratio between on-mound (see Table 3) and off-mound mean values (Table 4) during the same time period, i.e. duration of MFPs (factors presented in Fig. 3; note that factors were calculated for time equal intervals for each on-mound core individually and subsequently averaged). Due to the stratigraphic extent of the off-mound core, only the last two MFPs (MFP4 and MFP3) can be compared. During MFP4, on-mound carbon accumulation is higher by factors of 4.4–8.5, compared to the off-mound area; during MFP3 the factors range from 2.5 to 5.3 (Fig. 3). Generally, the same on-mound vs. off-mound relationship applies also to mound aggradation rates/sedimentation rates and carbonate accumulation rates (factors of 2.2–7.9 and 2.6–8.5, respectively). Across time, all rates are higher on the coral mounds.

In contrast, comparisons of the sediment carbon content (i.e. no timescale) reveal that the C_{inorg} content has an on-mound/off-mound ratio of ~ 1:1 throughout and that the off-mound is equally rich in carbonate (~ 86 wt.% during MFP3 and MFP4). The C_{org} content is more variable, with on- vs. off-mound factors of 0.9–1.5. Ultimately, if the carbon concentrations are added up together, the overall mean carbon concentration in the Campeche on-mound record (0.11 g C cm^{-3}; ± 0.02 SD) and the off-mound record (0.11 g C cm^{-3}; ± 0.01 SD) are virtually the same, with factors of 1.0–1.2 throughout. Hence, there are no major differences in overall carbon concentration between the mounds and the surrounding seabed (off-mound) in the Campeche Mound Province. Thus, the large differences between on- and off-mound deposition cannot be explained by differences in sediment composition, but only through the quantity of material deposited: It is merely the baffling capacity of a thriving CWC reef that causes the deposition and accumulation of the same material to happen at a much faster pace on the mound (see Wang et al. 2021). Beyond the stratigraphy of our records, this equally applies to the complete mound history since initiation, as reflected in the positive morphology of the mounds above the seafloor.

Despite low to moderate carbon accumulation (compared to other thriving coral mound provinces), limited siliciclastic sediment input in the region, and similar carbon concentrations on- and off-site, the living coral mound ecosystems of Campeche still effectively accumulate 3–9 times more carbon than the surrounding environment.

Carbon storage in the Campeche Mounds

Carbon accumulation in the Campeche Mounds has been investigated by combining two different approaches: the fully core-based and the mapping-based mound volume approach. The core-based approach relies on age models through coral dating to assign a time scale to carbon accumulation, and results in high-resolution data for distinct phases of mound formation. It quantifies the *process* of carbon accumulation locally, and its high temporal resolution facilitates the comparison with off-mound cores from the adjacent seafloor above. In contrast, the mapping-based approach quantifies the regional, mound province-wide net *product* of carbon accumulation. There, we present an estimate for the total carbon storage through combining a 3D mound volume analysis with the mean carbon concentration obtained from sediment cores. Carbon storage is here defined as the total amount of carbon stored throughout the existence of the Campeche coral mound ecosystems that has not been locally buried by equally carbon-rich sediments. This approach does not rely on core-specific aggradation rates. Nevertheless, in cases where the age of the mounds, i.e. its base, is known, this can be used to calculate spatially integrated net carbon accumulation rates (integrating over hiatuses in coral mound formation and local variabilities in coral mound aggradation). However, the mapping approach only allows to estimate the above-seafloor mound volumes. In many cases, coral mounds have considerable sub-seafloor extensions contributing significantly to the overall mound volume (e.g. Van Rooij et al. 2003; Hebbeln et al. 2019b). In this case, the Campeche Mounds are mostly exposed down to their base making their entire volume accountable for our approach. Further, while some coral mounds elsewhere exhibit inherited morphology growing on elevated volcanic ridges, the Campeche Mounds exhibit a self-developed morphology (sensu Wheeler et al. 2007; Tamborrino et al. 2022). The mound base is clearly formed by an extensive regional seismic reflector, indicating a very similar overall age for all the mounds (Hübscher et al. 2010; Hebbeln et al. 2014). This peculiar setting makes the Campeche Mounds suitable for volumetric upscaling.

The mean total carbon concentration of 0.11 g C_{total} cm^{-3} (± 0.02 SD) is considered a spatially and temporally representative value for the Campeche Mounds covering four MFPs from four different coral mound locations. Given the low variability in carbon concentration (± 16% rel. SD) throughout, the value can be reliably combined with the total mound volume to estimate the carbon stored in the Campeche Mounds. This is underlined by the fact that we found roughly consistent carbon accumulation characteristics across the mound province. Altogether, this additionally makes our core-based data suitable for volumetric upscaling. Furthermore, the volume estimate is fairly conservative, considering the exclusion of small features with height and width below the defined thresholds. The absolute amount of carbon stored through the mapped part of the Campeche Mound's ecosystems was estimated to be 18.5 Mt C_{total}. From that, the organic carbon fraction is estimated to be 0.6 Mt $C_{org.}$ This is an important, first estimate, filling a gap in our knowledge about long-term C_{org} burial in benthic ecosystems (Snelgrove et al. 2018).

Compared to the high age resolution core-based approach, the mapping approach accounts for spatial heterogeneity in mound morphology and therefore indirectly the variation in mound formation. While our volume-based mapping approach does not provide any detail on mound formation phases, it represents an estimate of the actual carbon storage since mound initiation. Yet, the exact timing of mound initiation in the Campeche Mound Province is unknown, as the material available for dating comes from our sediment cores that only penetrated the upper part of the mounds. The Campeche Mounds, however, emerge from a single regional seismic reflector (Hübscher et al. 2010; Hebbeln et al. 2014). This reflector is an unconformity with an estimated maximum age of 830 kyr, and a depositional system was re-established there ~ 570 kyr ago (Hübscher & Nürnberg 2023). This provides a clear indication that, in this region, coral mounds did not develop prior to ~ 830 kyr and no later than 570 kyr, which consequently are considered the maximum and minimum ages of the Campeche Mounds, respectively. With our mapping-based estimate of a total mean carbon storage of 18.5 Mt C, this results in a carbon accumulation of ~ 22,000–32,000 t C kyr^{-1}. If applied to the areal estimate from the mound delineation (total area covered by coral mounds: 16.7 km^2), we find a net carbon accumulation rate of 0.13–0.19 g C cm^{-2} kyr^{-1} since the initiation of mound formation in the Campeche Mound Province. This value lies just below the range of the mean overall surplus carbon accumulation values of 0.3–4.9 g C cm^{-2} kyr^{-1} determined from our sediment core-based analyses. The difference is mainly caused by the time averaging effect, as the mapping-based approach also interpolates over hiatuses, while the core-based approach only considers MFPs.

When comparing any accumulating systems, it is crucial to be aware of the timescales used. In this context, we provide two relevant numbers and timescales through this study: (1) the fully core-based, locally derived values for actively accumulating MFPs over relatively short time scales (~ 10 kyr), including the surplus carbon accumulation rate that describes how much additional carbon is accumulated through the mounds relative to the surrounding environment, and (2) the volume-derived all-time storage including accumulation rates accounting for periods of reef extinction or CWC absence, spatio-temporally averaged across the full area and large timescales (> 500 kyr). Most importantly, we suggest that the two rates resulting from these two approaches represent the maximum and the minimum of carbon accumulation within the Campeche Mounds. Notably, whereas the mound volume-based calculation represents the long-term net rate over various climate cycles and independent of fluctuations, the carbon accumulation through coral mounds can have a much higher regional importance at shorter timescales, during active mound formation.

Interestingly, Titschack et al. (2009), who investigated the carbonate accumulation of a large coral mound (Challenger Mound) in the Porcupine Seabight off Ireland, estimated the C_{inorg} accumulation of the last ~ 800 kyr in the Belgica Mound Province to be around ~ 0.7 g C_{inorg} cm^{-2} kyr^{-1}, which is ~ 3–5 times higher compared to our long-term rates for the Campeche Mounds. Hebbeln et al. (2019b) estimated a lower value of 0.04 g C_{inorg} cm^{-2} kyr^{-1} for the Atlantic Moroccan Coral Mound Province over the last ~ 900 kyr, which is ~ 3–5 times lower. This illustrates the regional variation of carbon accumulation for coral mounds, bearing in mind that these studies used less detailed estimates.

Further upscaling of the carbon storage through coral mound ecosystems is currently limited by a lack of data. The Campeche Mound Province is the only known coral mound province in the southern Gulf of Mexico, but the entire Yucatan Shelf margin provides overall suitable environmental conditions for reef-forming CWCs (Brooke et al. 2023), which is also supported by modelled projections (Cordes et al. 2023a). The Campeche Mound Province is likely larger than shown in this study, as its northern and southern boundaries are unknown (Hebbeln et al. 2012; 2014). We found evidence from a publicly available MBES data set (Hübscher 2022, available at: https://doi.org/10.1594/PANGAEA.950412) that the Campeche Mound Province extends a minimum of 13 km further south. This doubles the size of the Campeche Mound Province, and therefore the carbon storage is expected to be at least twice as high, i.e. ~ 37 Mt C or 44,000–64,000 t C kyr^{-1}. Lowery et al. (2024) also suggest the potential existence of coral mounds at slightly deeper waters downslope from our study site. Taking into account the above information, a similar sedimentary environment (Balsam and Beeson 2003), and historical point records of reef-building CWC species along the Campeche Bank margin (Schroeder et al. 2005; NOAA 2024; Freiwald et al. 2021), we can speculate as follows (see also Suppl. mat. VI): if only 1% of the Campeche Bank's slope between the 400 and 700 m depth isobath (i.e. ~ 10,200 km^2; based on GEBCO 2024) are covered by coral mounds with similar carbon accumulation characteristics, this would result in a carbon storage of 113 Mt C. This 1% estimate is fairly conservative, in contrast to the 12% coverage documented for the mapped Campeche Mound Province. As the mounds are currently in an active state, we can apply the mean values obtained from the cores for MFP4 to estimate a present-day carbon accumulation rate of ~ 2000–6000 t C per year. This amount of carbon is transferred into the lithosphere and fully immobilised for millions of years, thus, removed from the active, short-term carbon cycle (Zeebe 2012; Cartapanis et al. 2018).

Conclusion and outlook

With previous studies being limited to one mound, only one carbon source, short time periods, simplified assumptions and/or ex-situ data, we provide the most detailed estimate for carbon storage and accumulation in a coral mound province to date—and the first ones for the Gulf of Mexico and the West Atlantic—facilitated through a combination of a sediment core analyses *(1)* and a spatial mapping approach *(2)*. Through *(1)*, we document a carbon accumulation rate of 0.5–5.6 g C cm^{-2} kyr^{-1} for individual MFPs in the Campeche Mounds, which is effectively 3–9 times higher than the carbon accumulation at the surrounding seafloor—despite comparatively low to moderate mound aggradation rates, low sediment availability and no carbonate enrichment of the mounds. Through *(2)*, we integrate over extensive periods of reef growth and extinction, leading to an estimate for the long-term net total carbon accumulation rate of ~ 0.1–0.2 g C cm^{-2} kyr^{-1} for the Campeche Mounds. Together, they represent most certainly the upper and lower end of carbon accumulation rates in the Campeche Mounds, showcasing the range of values depending on the method and timescale analysed.

Overall, we document a total carbon storage of 18.5 Mt C in the Campeche Mounds. However, this may be much higher: suitable environmental conditions in this highly understudied region suggest that the Campeche Bank margin may be a hotspot for coral mound formation and benthic long-term carbon burial with regard to benthic deep-sea ecosystems worldwide.

Based on our conservative estimates, the Campeche Mounds do play a functional role in the long-term carbon cycle of the study area. As living ecosystems, their carbon accumulation rates lie in the same range as, for instance, long-term carbon accumulation rates from European Holocene peatlands (e.g. Longman et al. 2021; 2–12 g C cm^{-2} kyr^{-1}) or seagrass meadows (Apostolaki et al. 2024; 2–15 g C cm^{-2} kyr^{-1}; considering both organic and inorganic carbon).

On geological timescales, the reefs on the Campeche Mounds promote carbon storage, which can be considered an ecosystem service (sensu Costanza et al. 1997; Foley et al. 2010; Cordes et al. 2023b), underlining the importance of conservation for these ecosystems. In this context, Barnhill et al. (2022) emphasise the importance of integrating the quantification of dead material into holistic assessments of ecosystems and, ultimately, their value of preservation. As the Holocene is being replaced by the Anthropocene, changes in carbonate production and export due to ocean warming and acidification are projected to substantially affect carbonate burial dynamics of the southern Gulf of Mexico (Díaz-Ascencio et al. 2023), and ultimately, its CWC reefs. Effects of acidification on coral calcification and increased dissolution of CWC carbonate framework (Guinotte et al. 2006; Hennige et al. 2015; Büscher et al. 2017; 2019) will inevitably also alter carbon accumulation dynamics of the Campeche Mounds. Increases in dissolution rates to levels comparable to the North Pacific might prevent reef growth and mound formation in the future (e.g. Guinotte et al. 2006; Davies and Guinotte 2011). Further human impacts, such as destruction from deep-sea trawling (Hall-Spencer et al. 2002) or oil spills (Fisher et al. 2014) would additionally alter the Campeche CWC reef's ecosystem services. As recovery time of CWC reefs is slow (Clark et al. 2019; Bett et al. 2025), this is also relevant on geological timescales, and highlights the impact that human-induced global change may have on the large-scale functional role of benthic ecosystems in the carbon cycle.

Acknowledgements This study was funded by the Cluster of Excellence "The Ocean Floor – Earth's Uncharted Interface" [EXC-2077 – Grant 390741603 by Deutsche Forschungsgemeinschaft (DFG)]. Additionally, this study has received support from the DFG through funding of the "WACOM – West Atlantic Cold-water Coral Ecosystems project" [Grant HE 3412/17-1] and through providing ship time. L. Matos was supported by FCT Fundação para a Ciência e Tecnologia[SFRH/BD/72149/2010, UID/04326/2025 (https://doi.org/10.54499/UID/04326/2025), UID/PRR/04326/2025(https://doi.org/10.54499/UID/PRR/04326/2025) and LA/P/0101/2020 (https://doi.org/10.54499/LA/P/0101/2020)]. J. Titschack received support from the DFG project "Carbonate budget of cold-water coral mounds along a latitudinal transect" [DFG-Ti 706/1-1] to conduct CT measurements. We would like to thank Klinikum Bremen-Mitte, Christian Timann and Arne-Jörn Lemke for providing their facilities and their help for the performed computed tomographies. Riccardo Arosio, British Geological Survey, UK, is dearly thanked for his technical support using the CoMMa Toolbox. We would like to express our gratitude to René Eichstätter who sadly did not live to see the publication of his work, and Antonia Schafferts (both IUP Institute for Environmental Physics, University of Heidelberg, Germany), for their meticulous laboratory work on the Uranium-series dating of coral ages. We are highly grateful to Sina Franzen (University of Bremen, Germany) for assistance in CT data processing. We kindly acknowledge the GeoB Core Repository at MARUM (University of Bremen, Germany) for providing sediment cores and sample material, and Brit Kockisch, Christina Gnade and Timo Fleischmann (University of Bremen, Germany) for their help with sampling TIC/TOC and dry bulk density measurements. Further, the captain, crew, technicians and scientific party of the R/V Maria S. Merian cruise MSM20-4 (2012) are thanked for their assistance. Evan Edinger, Memorial University of Newfoundland, Canada, and one anonymous reviewer are greatly thanked for their input and for improving the quality of this paper. We highly appreciate Karla Rubio-Sandoval's (National Autonomous University of Mexico, Mexico City) role in naming the cold-water coral mounds: Ixchel, Ah Xoc and Chaac Mound were named after the local Mayan goddess of the moon and the tides, the god of water and the god of the sea, respectively. Ultimately, we are grateful to the Mexican Government for providing access to conduct scientific work in Mexican waters (Permit Number DGOPA-DAPA/2/1854/060312/475).

Author contribution DH conceptualised the study and acquired the project funding; JT, LDC and LG designed the methodology. DH and CW organised the data collection and, together with LM conducted the fieldwork. LM contributed further data sets used in the study. JT and LG performed the computed tomography measurements, LDC and JG supervised the mapping methodology and provided assistance in using the CoMMa Toolbox throughout. ASR, KA and NF performed the U-/Th-measurements and processed the coral age data. LG conducted the formal analysis, visualisation and wrote the original draft. All authors were involved in the interpretation of the results, the revision, and the writing of the final version of the paper.

Funding Open Access funding enabled and organized by Projekt DEAL.

Data availability Additional raw data information is provided in the Supplementary Information File. Data used for this study are openly available at the PANGAEA data repository, with computed tomography scan raw data of core GeoB16310-2: https://doi.org/10.1594/PANGAEA.980765;

GeoB16310-3: https://doi.org/10.1594/PANGAEA.981588; GeoB16313-2: https://doi.org/10.1594/PANGAEA.981823; GeoB16318-1: https://doi.org/10.1594/PANGAEA.982231. Processed computed tomography image-based volume data of core GeoB16318-1: https://doi.org/10.1594/PANGAEA.987046; GeoB16313-2: https://doi.org/10.1594/PANGAEA.987016; GeoB16310-3: https://doi.org/10.1594/PANGAEA.987010; GeoB16310-2: https://doi.org/10.1594/PANGAEA.987010. Sediment Density data are available for all on-mound cores via https://doi.org/10.1594/PANGAEA.986590, for the off-mound core GeoB16320-2 via https://doi.org/10.1594/PANGAEA.987077. Total organic carbon and total inorganic carbon content data of sediment core GeoB16320-2: https://doi.org/10.1594/PANGAEA.987071; GeoB16318-1; https://doi.org/10.1594/PANGAEA.987070; GeoB16313-2: https://doi.org/10.1594/PANGAEA.987069; GeoB16310-3: https://doi.org/10.1594/PANGAEA.987068; GeoB16310-2: https://doi.org/10.1594/PANGAEA.987056. Any further data sets are made available on request.

Any further data sets are made available on request.

Declarations

Competing interests The authors declare no competing interests.

References

Apostolaki ET, Lavery PS, Litsi-Mizan V, Serrano E, Inostroza K, Gerakaris V, Dailianis T, Glampedakis J, Holitzki T, Johnson E et al (2024) Patterns of Carbon and Nitrogen accumulation in seagrass (*Posidonia oceanica*) meadows of the Eastern Mediterranean Sea. J Geophys Res Biogeosci. https://doi.org/10.1029/2024jg008163

Arosio R, Gafeira J, De Clippele LH (2024a) CoMMa toolbox user guide Ver. 1.2. University College Cork, Marine Geosciences Research Group Cork, INFOMAR, British Geological Society & iAtlantic Project, Ireland

Arosio R, Gafeira J, De Clippele LH, Wheeler AJ, Huvenne VAI, Sacchetti F, Conti LA, Lim A (2024b) CoMMa: a GIS geomorphometry toolbox to map and measure confined landforms. Geomorphology. https://doi.org/10.1016/j.geomorph.2024.109227

Balsam WL, Beeson JP (2003) Sea-floor sediment distribution in the Gulf of Mexico. Deep Sea Res Part I Oceanogr Res Pap 50(12):1421–1444. https://doi.org/10.1016/j.dsr.2003.06.001

Barnhill KA, Roberts JM, Myers-Smith I, Williams M, Dexter KG, Ryan C, Wolfram U, Hennige SJ (2022) Incorporating dead material in ecosystem assessments and projections. Nat Clim Change 13(2):113–115. https://doi.org/10.1038/s41558-022-01565-5

Bett BJ, Piechaud N, Strong JA, Curtis EJ, Huvenne VAI (2025) Monitoring deep-sea cold-water coral ecosystems: 16-years of protection but no recovery on the Darwin Mounds (Bathyal NE Atlantic). Sci Total Environ 995:180118. https://doi.org/10.1016/j.scitotenv.2025.180118

Blaauw M, Christen JA (2011) Flexible paleoclimate age-depth models using an autoregressive gamma process. Bayesian Anal 6(3):457–474. https://doi.org/10.1214/11-BA618

Blum P (1997), Physical Properties Handbook: A Guide to the Shipboard Measurement of Physical Properties of Deep-Sea Cores. College Station, Texas, USA, http://www-odp.tamu.edu. Accessed 19 May 2025

Brooke S, Demopoulos A, Roberts H, Lunden J, Sutton T, and Davies A (2023), Cold-water corals of the world: Gulf of Mexico. In: Cold-Water Coral Reefs of the World, pp 51–90. https://doi.org/10.1007/978-3-031-40897-7_3

Büscher JV, Form AU, Riebesell U (2017) Interactive effects of ocean acidification and warming on growth, fitness and survival of the cold-water coral *Lophelia pertusa* under different food availabilities. Front Mar Sci. https://doi.org/10.3389/fmars.2017.00101

Büscher JV, Wisshak M, Form AU, Titschack J, Nachtigall K, Riebesell U (2019) In situ growth and bioerosion rates of *Lophelia pertusa* in a Norwegian fjord and open shelf cold-water coral habitat. PeerJ 7:e7586. https://doi.org/10.7717/peerj.7586

Butzin M, Köhler P, Lohmann G (2017) Marine radiocarbon reservoir age simulations for the past 50,000 years. Geophys Res Lett 44(16):8473–8480. https://doi.org/10.1002/2017gl074688

Cartapanis O, Galbraith ED, Bianchi D, Jaccard SL (2018) Carbon burial in deep-sea sediment and implications for oceanic inventories of carbon and alkalinity over the last glacial cycle. Clim past 14(11):1819–1850. https://doi.org/10.5194/cp-14-1819-2018

Cheng H, Lawrence Edwards R, Shen C-C, Polyak VJ, Asmerom Y, Woodhead J, Hellstrom J, Wang Y, Kong X, Spötl C et al (2013) Improvements in 230Th dating, 230Th and 234U half-life values, and U–Th isotopic measurements by multi-collector inductively coupled plasma mass spectrometry. Earth Planet Sci Lett 371–372:82–91. https://doi.org/10.1016/j.epsl.2013.04.006

Clark MR, Bowden DA, Rowden AA, Stewart R (2019) Little evidence of benthic community resilience to bottom trawling on seamounts after 15 years. Front Marine Sci 6:22. https://doi.org/10.3389/fmars.2019.00063

Corbera G, Lo Iacono C, Gràcia E, Grinyó J, Pierdomenico M, Huvenne VAI, Aguilar R, Gili JM (2019) Ecological characterisation of a Mediterranean cold-water coral reef: Cabliers coral mound Province (Alboran Sea, Western Mediterranean). Prog Oceanogr 175:245–262. https://doi.org/10.1016/j.pocean.2019.04.010

Corbera G, Lo Iacono C, Standish CD, Anagnostou E, Titschack J, Katsamenis O, Cacho I, Van Rooij D, Huvenne VAI, Foster GL (2021) Glacio-eustatic variations and sapropel events as main controls on the Middle Pleistocene-Holocene evolution of the Cabliers coral mound Province (W Mediterranean). Quat Sci Rev. https://doi.org/10.1016/j.quascirev.2020.106783

Cordes EE, Demopoulos AWJ, Davies AJ, Gasbarro R, Rhoads AC, Lobecker E, Sowers D, Chaytor JD, Morrison CL, Weinnig AM et al (2023c) Expanding our view of the cold-water coral niche and accounting of the ecosystem services of the reef habitat. Sci Rep 13(1):19482. https://doi.org/10.1038/s41598-023-45559-5

Cordes E, and Mienis F (eds) (2023). Cold-Water Coral Reefs of the World (Vol. 1). Springer Cham. https://doi.org/10.1007/978-3-031-40897-7

Cordes EE, Mienis F, Gasbarro R, Davies A, Baco AR, Bernardino AF, Clark MR, Freiwald A, Hennige SJ, Huvenne VAI et al. (2023a). A global view of the cold-water coral reefs of the world. In: Cold-Water Coral Reefs of the World, pp 1–30. https://doi.org/10.1007/978-3-031-40897-7_1

Correa TBS, Eberli GP, Grasmueck M, Reed JK, Correa AMS (2012) Genesis and morphology of cold-water coral ridges in a unidirectional current regime. Mar Geol 326–328:14–27. https://doi.org/10.1016/j.margeo.2012.06.008

Costanza R, d'Arge R, de Groot R, Farber S, Grasso M, Hannon B, Limburg K, Naeem S, O'Neill RV, Paruelo J, Raskin RG, Sutton P, van den Belt M (1997) The value of the world's ecosystem services and natural capital. Nature 387(6630):253–260. https://doi.org/10.1038/387253a0

Courtney TA, Andersson AJ (2025) Revisiting the terms used in net ecosystem calcification studies, carbonate budgets, and the equation of coral reef growth. Coral Reefs. https://doi.org/10.1007/s00338-025-02643-8

Creager JS (1959) Bathymetry and sediments of Bay of Campeche. Gulf Mexico AAPG Bull 43(7):1781–1781. https://doi.org/10.1306/0bda5e67-16bd-11d7-8645000102c1865d

Davies AJ, Guinotte JM (2011) Global habitat suitability for framework-forming cold-water corals. PLoS ONE 6(4):e18483. https://doi.org/10.1371/journal.pone.0018483

De Clippele LH, Gafeira J, Robert K, Hennige S, Lavaleye MS, Duineveld GCA, Huvenne VAI, Roberts JM (2017) Using novel acoustic and visual mapping tools to predict the small-scale spatial distribution oflive biogenic reef framework in cold-water coral habitats. Coral Reefs 36(1):255–268.https://doi.org/10.1007/s00338-016-1519-8

De Clippele LH, Rovelli L, Ramiro-Sánchez B, Kazanidis G, Vad J, Turner S, Glud RN, Roberts JM (2021a) Mapping cold-water coral biomass: an approach to derive ecosystem functions. Coral Reefs 40(1):215–231. https://doi.org/10.1007/s00338-020-02030-5

De Clippele LH, van der Kaaden A-S, Maier SR, de Froe E, Roberts JM (2021b) Biomass mapping for an improved understanding of the contribution of cold-water coral carbonate mounds to C and N cycling. Front Marine Sci. https://doi.org/10.3389/fmars.2021.721062

Díaz-Asencio M, Herguera JC, Romero FG, Rafter P (2023) Sediment accumulation rates and carbonate fluxes of deep-sea sediments in the southern Gulf of Mexico. Marine Geol. https://doi.org/10.1016/j.margeo.2023.107131

Domínguez Castanedo N, Hernández Alcántara P, Solís-Weiss V, Granados Barba A (2012) Distribution of polychaete feeding guilds in sedimentary environments of the Campeche Bank, Southern Gulf of Mexico. Helgol Mar Res 66(4):469–478. https://doi.org/10.1007/s10152-011-0283-y

Dorschel B, Hebbeln D, Rüggeberg A, Dullo C (2007) Carbonate budget of a cold-water coral carbonate mound: Propeller Mound, Porcupine Seabight. Int J Earth Sci 96(1):73–83. https://doi.org/10.1007/s00531-005-0493-0

Edinger E, Bourillet J.-F, Menot L, Lartaud F, Chemel M, and Jorry S (2025). Late Holocene and recent cold-water coral calcium carbonate production in Guilvinec Canyon, Bay of Biscay, France. Deep Sea Research Part II: Topical Studies in Oceanography, 220. https://doi.org/10.1016/j.dsr2.2024.105451

Fink HG, Wienberg C, De Pol-Holz R, Wintersteller P, Hebbeln D (2013) Cold-water coral growth in the Alboran Sea related to high productivity during the Late Pleistocene and Holocene. Mar Geol 339:71–82. https://doi.org/10.1016/j.margeo.2013.04.009

Fisher CR, Hsing PY, Kaiser CL, Yoerger DR, Roberts HH, Shedd WW, Cordes EE, Shank TM, Berlet SP, Saunders, et al (2014) Footprint of Deepwater Horizon blowout impact to deep-water coral communities. Proc Natl Acad Sci USA 111(32):11744–11749. https://doi.org/10.1073/pnas.1403492111

Foley NS, van Rensburg TM, Armstrong CW (2010) The ecological and economic value of cold-water coral ecosystems. Ocean Coast Manag 53(7):313–326. https://doi.org/10.1016/j.ocecoaman.2010.04.009

Frank N, Paterne M, Ayliffe L, van Weering T, Henriet J-P, Blamart D (2004) Eastern North Atlantic deep-sea corals: tracing upper intermediate water $\Delta^{14}C$ during the Holocene. Earth Planet Sci Lett 219(3–4):297–309. https://doi.org/10.1016/s0012-821x(03)00721-0

Freiwald A, Fosså JH, Grehan A, Koslow T, and Roberts JM (2004), Cold-water coral reefs: out of sight-no longer out of mind. UNEP-WCMC.

Freiwald A, Rogers A, Hall-Spencer J, Guinotte JM, Davies AJ, Yesson C, Martin CS, and Weatherdon LV (2021), Global distribution of cold-water corals (version 5.1). Fifth update to the dataset in Freiwald et al. (2004) by UNEP-WCMC, in collaboration with Andre Freiwald and John Guinotte. In. Cambridge, UK: UN Environment Programme World Conservation Monitoring Centre. https://doi.org/10.34892/72x9-rt61

Friedlingstein P, O'Sullivan M, Jones MW, Andrew RM, Hauck J, Landschützer P, Le Quéré C, Li H, Luijkx IT, Olsen A et al (2025) Global Carbon Budget 2024. Earth Syst Sci Data 17(3):965–1039. https://doi.org/10.5194/essd-17-965-2025

Gafeira J, Arosio R, and De Clippele LH (2024), CoMMa: CoMMa Toolbox v1.2 (CoMMa1_2). Zenodo. https://doi.org/10.5281/zenodo.11109024 [software]

Gafeira J, Dolan MFJ, Monteys X (2018) Geomorphometric characterization of pockmarks by using a GIS-based semi-automated toolbox. Geosciences. https://doi.org/10.3390/geosciences8050154

Gafeira J, Long D, Diaz-Doce D (2012) Semi-automated characterisation of seabed pockmarks in the centralNorth Sea. Near Surf Geophys 10(4):301–312. https://doi.org/10.3997/1873-0604.2012018

GEBCO Bathymetric Compilation Group (2024) The GEBCO_2024 Grid – a continuous terrain model of the global oceans and land. NERC EDS Br Oceanogr Data Centre. https://doi.org/10.5285/1c44ce99-0a0d-5f4f-e0637086abc0ea0f

Greiffenhagen L, Titschack J, Wienberg C, Wang H, Hebbeln D (2025a) Cold-water coral mounds are effective carbon sinks in the western Mediterranean Sea. Biogeosciences 22(9):2201–2223. https://doi.org/10.5194/bg-22-2201-2025

Greiffenhagen L, Titschack J, Wienberg C, Hebbeln D, Timann C, Lemke A-J (2025b), CT raw data (DICOM format) of sediment core GeoB16310-2 from the Campeche Cold-water coral mounds, Maria S. Merian cruise MSM20-4 . PANGAEA, https://doi.pangaea.de/10.1594/PANGAEA.980765

Guinotte JM, Orr J, Cairns S, Freiwald A, Morgan L, George R (2006) Will human-induced changes in seawater chemistry alter the distribution of deep-sea scleractinian corals? Front Ecol Environ 4(3):141–146. https://doi.org/10.1890/1540-9295(2006)004[0141:Whcisc]2.0.Co;2

Hall-Spencer J, Allain V, Fosså JH (2002) Trawling damage to Northeast Atlantic ancient coral reefs. Proc Biol Sci 269(1490):507–511. https://doi.org/10.1098/rspb.2001.1910

Hebbeln D, Wienberg C, Wintersteller P, Freiwald A, Becker M, Beuck L, Dullo C, Eberli GP, Glogowski S, Matos L et al (2014) Environmental forcing of the Campeche cold-water coral province, southern Gulf of Mexico. Biogeosciences 11(7):1799–1815. https://doi.org/10.5194/bg-11-1799-2014

Hebbeln D, Van Rooij D, Wienberg C (2016) Good neighbours shaped by vigorous currents: cold-water coral mounds and contourites in the North Atlantic. Mar Geol 378:171–185. https://doi.org/10.1016/j.margeo.2016.01.014

Hebbeln D, Bender M, Gaide S, Titschack J, Vandorpe T, Van Rooij D, Wintersteller P, Wienberg C (2019b) Thousands of cold-water coral mounds along the Moroccan Atlantic continental margin: distribution and morphometry. Mar Geol 411:51–61. https://doi.org/10.1016/j.margeo.2019.02.001

Hebbeln D, Wienberg C and Cruise Participants (2012), Report and preliminary results of R/V Maria S. Merian cruise MSM20–4. WACOM – West-Atlantic Cold-water Corals Ecosystems: The West Side Story. Bridgetown – Freeport, 14 March – 7 April 2012. MARUM Berichte, MARUM – Zentrum für Marine

Umweltwissenschaften, Fachbereich Geowissenschaften, Universität Bremen, No. 290, 120 pp.
Hebbeln D, Portilho-Ramos RDC, Wienberg C, Titschack J (2019a) The fate of cold-water corals in a changing world: a geological perspective. Front Marine Sci. https://doi.org/10.3389/fmars.2019.00119
Hennige SJ, Wicks LC, Kamenos NA, Perna G, Findlay HS, Roberts JM (2015) Hidden impacts of ocean acidification to live and dead coral framework. Proc Biol Sci 282(1813):20150990. https://doi.org/10.1098/rspb.2015.0990
Holmes CW (1976) Distribution, regional variation, and geochemical coherence of selected elements in the sediments of the central Gulf of Mexico. Report. https://doi.org/10.3133/pp928
CHübscher2022Multibeam bathymetry processed data (EM 120 echosounder working area dataset) of RV METEOR during cruise M94, eastern Campeche BankGulf of Mexico PANGAEA10.1594/PANGAEA.950412Hübscher C (2022) Multibeam bathymetry processed data (EM 120 echosounder working area dataset) of RV METEOR during cruise M94, eastern Campeche Bank. Gulf of Mexico PANGAEA. https://doi.org/10.1594/PANGAEA.950412
Hübscher C, Dullo C, Flögel S, Titschack J, Schönfeld J (2010) Contourite drift evolution and related coral growth in the eastern Gulf of Mexico and its gateways. Int J Earth Sci 99(S1):191–206. https://doi.org/10.1007/s00531-010-0558-6
Hübscher C, Nürnberg D (2023) Loop Current attenuation after the Mid-Pleistocene Transition contributes to Northern hemisphere cooling. Marine Geol. https://doi.org/10.1016/j.margeo.2022.106976
Kano A, Ferdelman TG, Williams T, Henriet J-P, Ishikawa T, Kawagoe N, Takashima C, Kakizaki Y, Abe K, Sakai S et al (2007) Age constraints on the origin and growth history of a deep-water coral mound in the Northeast Atlantic drilled during Integrated Ocean Drilling Program Expedition 307. Geology. https://doi.org/10.1130/g23917a.1
Kerber IK, Arps J, Eichstädter R, Kontor F, Dornick C, Schröder-Ritzrau A, Babu A, Warken S, Frank N (2023) Simultaneous U and Th isotope measurements for U-series dating using MCICPMS. Nucl Instrum Methods Phys Res B Beam Interact Mater Atoms 539:169–178. https://doi.org/10.1016/j.nimb.2023.04.003
Kerber IK, Kontor F, Mielke A, Warken S, Frank N (2025) Technical note: “U–Th Analysis” – open-source softwarededicated to MC-ICP-MS U-series data treatment and evaluation. Geochronology, 7(1):1–13. https://doi.org/10.5194/gchron-7-1-2025
Kim SS, Wessel P (2008) Directional median filtering for regional-residual separation of bathymetry. Geochem Geophys Geosyst. https://doi.org/10.1029/2007gc001850
Kiriakoulakis K, Freiwald A, Fisher E, Wolff GA (2007) Organic matter quality and supply to deep-water coral/mound systems of the NW European Continental Margin. Int J Earth Sci 96(1):159–170. https://doi.org/10.1007/s00531-006-0078-6
Langner M, Mulitza S (2019) Technical note: PaleoDataView – a software toolbox for the collection, homogenization and visualization of marine proxy data. Clim past 15(6):2067–2072. https://doi.org/10.5194/cp-15-2067-2019
Lindberg B, Mienert J (2005) Postglacial carbonate production by cold-water corals on the Norwegian Shelf and their role in the global carbonate budget. Geology. https://doi.org/10.1130/g21577.1
Lindsay JB, Cockburn JMH, Russell HAJ (2015) An integral image approach to performing multi-scale topographic position analysis. Geomorphology 245:51–61. https://doi.org/10.1016/j.geomorph.2015.05.025
Longman J, Veres D, Haliuc A, Finsinger W, Ersek V, Pascal D, Sava T, Begy R (2021) Carbon accumulation rates of Holocene peatlands in central–eastern Europe document the driving role of human impact over the past 4000 years. Clim past 17(6):2633–2652. https://doi.org/10.5194/cp-17-2633-2021
Lowery CM, Perez Cruz L, Urrutia Fucugauchi J, Wei J, Austin JA, Standring P (2024) Seismic stratigraphy of contourite drift deposits associated with the Loop Current on the Eastern Campeche Bank, Gulf of Mexico. Paleoceanogr Paleoclimatol. https://doi.org/10.1029/2023pa004701
Lunden JJ, Georgian SE, Cordes EE (2013) Aragonite saturation states at cold-water coral reefs structured by *Lophelia pertusa* in the northern Gulf of Mexico. Limnol Oceanogr 58(1):354–362. https://doi.org/10.4319/lo.2013.58.1.0354
Maier SR, Brooke S, De Clippele LH, de Froe E, van der Kaaden AS, Kutti T, Mienis F, van Oevelen D (2023) On the paradox of thriving cold-water coral reefs in the food-limited deep sea. Biol Rev Camb Philos Soc. https://doi.org/10.1111/brv.12976
Matos L, Wienberg C, Titschack J, Schmiedl G, Frank N, Abrantes F, Cunha MR, Hebbeln D (2017) Coral mound development at the Campeche cold-water coral province, southern Gulf of Mexico: implications of Antarctic Intermediate Water increased influence during interglacials. Mar Geol 392:53–65. https://doi.org/10.1016/j.margeo.2017.08.012
Merino M (1997) Upwelling on the Yucatan Shelf: hydrographic evidence. J Mar Syst 13(1):101–121. https://doi.org/10.1016/S0924-7963(96)00123-6
Meunier T, Le Boyer A, Molodtsov S, Bower A, Furey H, Robbins P (2023) Internal wave activity in the deep Gulf of Mexico. Front Mar Sci. https://doi.org/10.3389/fmars.2023.1285303
Mienis F, van Weering T, de Haas H, de Stigter H, Huvenne V, Wheeler A (2006) Carbonate mound development at the SW Rockall Trough margin based on high resolution TOBI and seismic recording. Mar Geol 233(1):1–19. https://doi.org/10.1016/j.margeo.2006.08.003
Mienis F, van der Land C, de Stigter HC, van de Vorstenbosch M, de Haas H, Richter T, van Weering TCE (2009) Sediment accumulation on a cold-water carbonate mound at the Southwest Rockall Trough margin. Mar Geol 265(1–2):40–50. https://doi.org/10.1016/j.margeo.2009.06.014
Mienis F, Duineveld GCA, Davies AJ, Ross SW, Seim H, Bane J, van Weering TCE (2012) The influence of near-bed hydrodynamic conditions on cold-water corals in the Viosca Knoll area, Gulf of Mexico. Deep Sea Res Part I Oceanogr Res Pap 60:32–45. https://doi.org/10.1016/j.dsr.2011.10.007
NOAA. (2024). National Database for Deep-Sea Corals and Sponges, Portal Ver. 3.0.1. https://www.ncei.noaa.gov/maps/deep-sea-corals-portal/. Accessed 19 May 2025 [DATABASE]
Orsi TH, Edwards CM, Anderson AL (1994) X-ray computed tomography: a nondestructive method for quantitative analysis of sediment cores. J Sediment Res. https://doi.org/10.1306/D4267E74-2B26-11D7-8648000102C1865D
Portilho-Ramos RDC, Titschack J, Wienberg C, Siccha Rojas MG, Yokoyama Y, Hebbeln D (2022) Major environmental drivers determining life and death of cold-water corals through time. PLoS Biol 20(5):e3001628. https://doi.org/10.1371/journal.pbio.3001628
Raddatz J, Titschack J, Frank N, Freiwald A, Conforti A, Osborne A, Skornitzke S, Stiller W, Rüggeberg A, Voigt S, Albuquerque ALS, Vertino A, Schröder-Ritzrau A, Bahr A (2020) *Solenosmilia variabilis*-bearing cold-water coral mounds off Brazil. Coral Reefs 39(1):69–83. https://doi.org/10.1007/s00338-019-01882-w
Reijmer JJG (2021) Marine carbonate factories: review and update. Sedimentology 68(5):1729–1796. https://doi.org/10.1111/sed.12878
Reimer PJ, Austin WEN, Bard E, Bayliss A, Blackwell PG, Bronk Ramsey C, Butzin M, Cheng H, Edwards RL, Friedrich M et al (2020) The IntCal20 Northern Hemisphere radiocarbon age

calibration curve (0–55 cal kBP). Radiocarbon 62(4):725–757. https://doi.org/10.1017/rdc.2020.41
Reyes-Jiménez T, Athié G, Enriquez C, Sheinbaum J, Mariño-Tapia I, Marín-Hernández M, Salas-Monreal D, Candela J (2023) Triggering mechanisms of the Yucatan upwelling. Cont Shelf Res. https://doi.org/10.1016/j.csr.2022.104910
Roberts JM, Freiwald A, Wheeler A, and Cairns S (2009), Reefs and mounds. In: Cold-Water Corals. Cambridge University Press, pp 108–141. https://doi.org/10.1017/cbo9780511581588.005
Roberts HH, Kohl B (2018) Temperature control of cold-water coral (*Lophelia*) mound growth by climate-cycle forcing, Northeast Gulf of Mexico. Deep Sea Res Part I Oceanogr Res Pap 140:142–158. https://doi.org/10.1016/j.dsr.2018.08.002
Schlager W (2003) Benthic carbonate factories of the Phanerozoic. Int J Earth Sci 92(4):445–464. https://doi.org/10.1007/s00531-003-0327-x
Schönfeld J (2010), CaCO3 concentrations of sediment core M78/1_180-1 PANGAEA. https://doi.org/10.1594/PANGAEA.740018
Schroeder WW, Brooke SD, Olson JB, Phaneuf B, McDonough JJ, Etnoyer P (2005) Occurrence of deep-water *Lophelia pertusa* and *Madrepora oculata* in the Gulf of Mexico. In: Freiwald A, Roberts JM (eds) Cold-water corals and ecosystems. Springer, Berlin Heidelberg, pp 297–307. https://doi.org/10.1007/3-540-27673-4_14
Schultz C, Luo JY, Brady DC, Fulweiler RW, Long MH, Petrik CM, Testa JM, Benway HM, Burdige D, Cecchetto MM et al (2025) Elucidating the role of marine benthic carbon in a changing world. Glob Biogeochem Cycles. https://doi.org/10.1029/2025gb008643
Smith SV, Mackenzie FT (2015) The role of $CaCO_3$ reactions in the contemporary oceanic CO_2 cycle. Aquat Geochem 22(2):153–175. https://doi.org/10.1007/s10498-015-9282-y
Smith MJ, Rose J, Gousie MB (2009) The cookie cutter: a method for obtaining a quantitative 3D description of glacial bedforms. Geomorphology 108(3–4):209–218. https://doi.org/10.1016/j.geomorph.2009.01.006
Snelgrove PVR, Soetaert K, Solan M, Thrush S, Wei CL, Danovaro R, Fulweiler RW, Kitazato H, Ingole B, Norkko A et al (2018) Global carbon cycling on a heterogeneous seafloor. Trends Ecol Evol 33(2):96–105. https://doi.org/10.1016/j.tree.2017.11.004
Sowers DC, Mayer LA, Masetti G, Cordes E, Gasbarro R, Lobecker E, Cantwell K, Candio S, Hoy S, Malik M et al (2024) Mapping and geomorphic characterization of the vast cold-water coral mounds of the Blake Plateau. Geomatics 4(1):17–47. https://doi.org/10.3390/geomatics4010002
Stalling D, Westerhoff M, and Hege H-C (2005), Amira: a highly interactive system for visual data analysis, In: Hansen CD and Johnson CR (eds) Visualization Handbook, Butterworth-Heinemann, pp 749–767, https://doi.org/10.1016/B978-0123875822/50040-X
Steinmann L, Baques M, Wenau S, Schwenk T, Spiess V, Piola AR, Bozzano G, Violante R, Kasten S (2020) Discovery of a giant cold-water coral mound province along the northern Argentine margin and its link to the regional Contourite Depositional System and oceanographic setting. Marine Geol 427:11. https://doi.org/10.1016/j.margeo.2020.106223
Tamborrino L, Titschack J, Wienberg C, Purkis S, Eberli GP, Hebbeln D (2022) Spatial distribution and morphometry of the Namibian coral mounds controlled by the hydrodynamic regime and outer-shelf topography. Front. Marine Sci. 9:22. https://doi.org/10.3389/fmars.2022.877616
Titschack J, Thierens M, Dorschel B, Schulbert C, Freiwald A, Kano A, Takashima C, Kawagoe N, Li X (2009) Carbonate budget of a cold-water coral mound (Challenger Mound, IODP Exp. 307). Mar Geol 259(1–4):36–46. https://doi.org/10.1016/j.margeo.2008.12.007
Titschack J, Baum D, De Pol-Holz R, López Correa M, Forster N, Flögel S, Hebbeln D, Freiwald A (2015) Aggradation and carbonate accumulation of Holocene Norwegian cold-water coral reefs. Sedimentology 62(7):1873–1898. https://doi.org/10.1111/sed.12206
Titschack J, Fink HG, Baum D, Wienberg C, Hebbeln D, Freiwald A (2016) Mediterranean cold-water corals – an important regional carbonate factory? Depos Rec 2(1):74–96. https://doi.org/10.1002/dep2.14
Titschack, J, Timann, C, Lemke, A-J (2025a), CT raw data (DICOM format) of coral mound core GeoB16310-3 from the Campeche coral mound province, Maria S. Merian cruise MSM20-4. PANGAEA, https://doi.pangaea.de/10.1594/PANGAEA.981588
Titschack, J, Timann C, Lemke A-J (2025b), CT raw data (DICOM format) of coral mound core GeoB16313-2 from the Campeche coral mound province, Maria S. Merian cruise MSM20-4. PANGAEA, https://doi.pangaea.de/10.1594/PANGAEA.981823
Titschack J, Timann C, Lemke A-J (2025c), CT raw data (DICOM format) of coral mound core GeoB16318-1 from the Campeche coral mound province, Maria S. Merian cruise MSM20-4 . PANGAEA, https://doi.pangaea.de/10.1594/PANGAEA.982231
Van Rooij D, De Mol B, Huvenne V, Ivanov M, Henriet JP (2003) Seismic evidence of current-controlled sedimentation in the Belgica mound province, upper Porcupine slope, southwest of Ireland. Mar Geol 195(1):31–53. https://doi.org/10.1016/S0025-3227(02)00681-3
Wang H, Titschack J, Wienberg C, Korpanty C, Hebbeln D (2021) The importance of ecological accommodation space and sediment supply for cold-water coral mound formation, a case study from the Western Mediterranean Sea. Front Marine Sci. https://doi.org/10.3389/fmars.2021.760909
Wefing A-M, Arps J, Blaser P, Wienberg C, Hebbeln D, Frank N (2017) High precision U-series dating of scleractinian cold-water corals using an automated chromatographic U and Th extraction. Chem Geol 475:140–148. https://doi.org/10.1016/j.chemgeo.2017.10.036
Wheeler AJ, Beyer A, Freiwald A, de Haas H, Huvenne VAI, Kozachenko M, Olu-Le Roy K, Opderbecke J (2007) Morphology and environment of cold-water coral carbonate mounds on the NW European margin. Int J Earth Sci 96(1):37–56. https://doi.org/10.1007/s00531-006-0130-6
Wienberg C, Titschack J, Freiwald A, Frank N, Lundälv T, Taviani M, Beuck L, Schröder-Ritzrau A, Krengel T, Hebbeln D (2018) The giant Mauritanian cold-water coral mound province: oxygen control on coral mound formation. Quat Sci Rev 185:135–152. https://doi.org/10.1016/j.quascirev.2018.02.012
Wienberg C, Krengel T, Frank N, Wang H, Van Rooij D, Hebbeln D (2022) Cold-water coral mounds in the Western Mediterranean Sea: new insights into their initiation and development since the Mid-Pleistocene in response to changes of African hydroclimate. Quat Sci Rev. https://doi.org/10.1016/j.quascirev.2022.107723
Wienberg C, and Titschack J (2017). Framework-forming scleractinian cold-water corals through space and time: a late quaternary North Atlantic perspective. In Rossi S, Bramanti L, Gori A, and Orejas C (Eds.), Marine Animal Forests (pp 699–732). https://doi.org/10.1007/978-3-319-17001-5_16-1
Wilhelm O, Ewing M (1972) Geology and history of the Gulf of Mexico. Geol Soc Am Bull 83(3):575–600. https://doi.org/10.1130/0016-7606(1972)83[575:Gahotg]2.0.Co;2
Wintersteller P, and Eberli GP (2019), Gridded bathymetry from EM120 multibeam echosounder of RV Maria S. Merian cruise MSM20/4 (Florida Strait, Caribbean) PANGAEA. https://doi.org/10.1594/PANGAEA.902472
Wood M, Hayes CT, Paytan A (2023) Global Quaternary carbonate burial: proxy- and model-based reconstructions and persisting

uncertainties. Ann Rev Mar Sci 15:277–302. https://doi.org/10.1146/annurev-marine-031122-031137

Zeebe RE (2012) History of seawater carbonate chemistry, atmospheric CO_2, and ocean acidification. Annu Rev Earth Planet Sci 40(1):141–165. https://doi.org/10.1146/annurev-earth-042711-105521